LATVIJAS UNIVERSITĀTE

UNIVERSITY OF LATVIA

LIĀNA ŠIRMANE

NANOSTRUKTURĒTU KOMPLEKSO OKSĪDU LUMINOFORU VAKUUMA ULTRAVIOLĒTAS IEROSMES SPEKTROSKOPIJA

VACUUM ULTRAVIOLET EXCITATION SPECTROSCOPY OF NANOSTRUCTURED COMPLEX OXIDE PHOSPHORS

Zinātnisko publikāciju kopa

Scientific papers

Rīga, 2017

Anotācija

Perspektīvākais luminiscences nanomateriālu pielietojums ir saistīts ar medicīnu un molekulāro bioloģiju. Medicīniskajā diagnostikā un terapijā luminiscences nanomateriāli ir daudzsološi marķieri optiskajā attēlveidošanā un luminiscējošā iezīmēšanā, kas ļauj izmantot jaunas neinvazīvas diagnostikas metodes un kompleksas vitālās funkcijas *in vivo* novērošanu. Šajā darbā ir izveidots aktuālo nanoizmēru luminiscences komplekso oksīdu ($LaPO_4$:Ce,Tb; YVO_4:Eu; $Y_3Al_5O_{12}$:Ce (YAG:Ce); $ZnWO_4$; $NiWO_4$) sistemātiska spektroskopiska pētījuma kopsavilkums ar mērķi, izmantojot luminiscences spektroskopiju ar enerģijas un laika izšķiršanu, izanalizēt elektronu relaksācijas procesus. Eksperimenti ir veikti, izmantojot Eiropas sinhrotronu centrus: 1) Superlumi galastaciju uz eksperimentālās līnijas I pie DORIS III uzglabāšanas gredzena DESY sinhrotronā (Hamburgā, Vācijā); 2) FinEst ondulatoru luminiscences galastaciju pie MAX III uzglabāšanas gredzena MAX IV sinhrotronā (Lundā, Zviedrijā). Pētījumi ir fokusēti uz enerģijas pārneses procesiem retzemju jonu optiskajās pārejās. Lai sniegtu papildu informāciju par elektronu struktūru un elektronu ierosmi nanofosforos, tiek aplūkota dažādu parametru, piemēram, temperatūras, piemaisījuma jonu koncentrācijas un sākotnējā ierosinātā stāvokļa ietekme. Darbā ir konstatēta ievērojama atšķirība luminiscences īpašībās starp nano un makroskopiskiem analogiem. Iegūtie rezultāti parāda, ka mazs nanodaļiņu izmērs un nanodaļiņu virsma ir atbildīgi par izmaiņām nanoizmēru komplekso oksīdu luminiscences īpašībās.

Abstract

The most ambitious and fascinating application of luminescent nanomaterials is probably related to medicine and molecular biology. Here, luminescent nanomaterials are promising tags for optical imaging and fluorescent labelling to allow for novel techniques of non-invasive diagnosis and *in vivo* observation of complex vital functions. The current work is a summary of the systematic spectroscopic studies of actual nanosized luminescent complex oxides ($LaPO_4$:Ce,Tb; YVO_4:Eu; $Y_3Al_5O_{12}$:Ce (YAG:Ce); $ZnWO_4$; $NiWO_4$) with an attempt to analyse the electronic relaxation processes performed using energy and time-resolved luminescence spectroscopy. The experiments have been carried out utilising European synchrotron centres: i) The Superlumi endstation of I3 line of DORIS III storage ring at DESY (Hamburg, Germany); ii) The luminescence endstation of the FinEst undulator beamline of MAX III storage ring at MAX IV (Lund, Sweden). The examinations focused on the energy transfer processes within the rare-earth ions leading to the optical transitions. The influence of the different parameters such as temperature, doping concentration, and initial excited state were treated to provide complementary information concerning the electronic structure as well as electronic excitations in nanophosphors. A significant difference in luminescence properties between the nano and macroscopical analogues was found in the current work. The results achieved show that small nanoparticle size and loss centres related to the surface of a nanoparticle are responsible for changes in the luminescence properties of nanosized complex oxides.

Promocijas darbā iekļauto publikāciju saraksts

List of scientific papers included in the Thesis

P1 V. Pankratov, A.I. Popov, **L. Shirmane**, A. Kotlov, C. Feldmann, $LaPO_4$:Ce, Tb and YVO_4:Eu nanophosphors: Luminescence studies in the vacuum ultraviolet spectral range, *Journal of Applied Physics* **110** (2011) 053522

P2 **L. Shirmane**, C. Feldmann, V. Pankratov, Comparing the Luminescence Processes of YVO_4:Eu and core-shell YVO_4@YF_3 Nanocrystals with Bulk-YVO_4:Eu, *Physica B: Condensed Matter* **504** (2017) 80-85

P3 **L. Shirmane**, V. Pankratov, Emerging blue-UV luminescence in cerium doped YAG nanocrystals, *Physica Status Solidi – Rapid Research Letters* **10** (2016) 475-479

P4 A. Kalinko, A. Kotlov, A. Kuzmin, V. Pankratov, A. I. Popov, **L. Shirmane**, Electronic excitation in $ZnWO_4$ and $Zn_cNi_{1-c}WO_4$ using VUV synchrotron radiation, *Central European Journal of Physics* **9** (2011) 432-437

P5 A. Kuzmin, V. Pankratov, A. Kalinko, A. Kotlov, **L. Shirmane**, A.I. Popov, UV-VUV synchrotron radiation spectroscopy of $NiWO_4$, *Low Temperature Physics* **42** (2016) 543-546

$LaPO_4$:Ce,Tb and YVO_4:Eu nanophosphors: Luminescence studies in the vacuum ultraviolet spectral range

V. Pankratov,[1,a] A. I. Popov,[1,2] L. Shirmane,[1] A. Kotlov,[3] and C. Feldmann[4]
[1]*Institute of Solid State Physics, University of Latvia, 8 Kengaraga, Riga LV-1063, Latvia*
[2]*Institute Laue Langevin, 6 rue Jule Horovitz, Grenoble 38042, France*
[3]*HASYLAB at DESY, Notkestrasse 85, Hamburg D-22607, Germany*
[4]*Institute of Inorganic Chemistry, Karlsruhe Institute of Technology (KIT), Engesserstrasse 15, Karlsruhe D-76131, Germany*

(Received 16 June 2011; accepted 5 August 2011; published online 14 September 2011)

Comparative analysis of the luminescent properties of nanocrystalline $LaPO_4$:Ce,Tb and YVO_4:Eu luminescent materials with macrocrystalline analogues, commercially produced by Philips, has been performed under excitation by pulsed vacuum ultraviolet (VUV) synchrotron radiation, ranging from 3.7-40 eV. Special attention was paid to VUV spectral range, which is not reachable with commonly used lamp and laser sources. Our results clearly show distinct difference in the excitation spectra for nano- and macrocrystalline samples, especially at energies, when the spatial separation of electron-hole pairs is comparable with sizes of nanoparticles. Differences in the region of multiplication of the electronic excitations are also demonstrated and discussed. © *2011 American Institute of Physics*. [doi:10.1063/1.3634112]

I. INTRODUCTION

Oxide luminescent materials $LaPO_4$ and YVO_4 doped with lanthanide ions have been extensively studied as prospective materials in the fields of high-resolution optical devices, such as color television cathode ray tubes, high-pressure mercury lamps, electroluminescent and field emission displays, or as nanophosphors for biological labeling and bifunctional magnetic-luminescent nanocomposites.[1–16] These phosphors are characterized by their high energy-conversion efficiency, purity in spectral colors, and high thermal stability. They have the advantage over the currently used sulfide phosphors in stability in vacuum and absence of corrosive gas emission under electron bombardment.[17]

One of the materials discussed in this paper is YVO_4:Eu. Since Levine and Palilla[1] in 1964 developed the Eu^{3+}-doped YVO_4 as a red phosphor for the commercial applications in color television cathode ray tube displays and high-pressure mercury lamps, there has been extensive study on this material doped with different lanthanide ions, such as Er^{3+}, Sm^{3+}, and Dy^{3+}. Luminescence properties of YVO_4:Eu^{3+} crystals and related materials have been studied for more than three decades.[1–3,6,7,15,18–21] The absorption spectrum of YVO_4 shows strong and broad bands in the ultraviolet (UV) region. The absorption transition involved is a charge transfer from oxygen 2p to the vanadium 3d states, forming excited $(VO_4)^{3-}$ molecular complex. Considerably small Stokes shift of the emission from such $(VO_4)^{3-}$ vanadate group leads to favorable conditions for thermally activated energy migration. Thus, bulk YVO_4:Eu^{3+} shows strong red emission under UV illumination due to efficient energy transfer from excited $(VO_4)^{3-}$ complex anions to Eu^{3+} activator ions. Quantum yields as high as 70% are reported, providing the bulk YVO_4:Eu^{3+} material as one of the most important phosphor compounds.

In 1998, Hasse and Riwotzki first applied the hydrothermal method in the synthesis of lanthanide-doped YVO_4 nanocrystalline powers, which were weakly dispersed as an aqueous colloid.[3] In 2000, Huignard *et al.*[6] gained the concentrated colloidal solutions of well-dispersed YVO_4:Eu^{3+} nanoparticles by precipitation reactions at room temperature. Later, they synthesized colloidal YVO_4:Eu^{3+} nanoparticles with a diameter of $\sim$8 nm,[7] and in the colloids, the YVO_4:Eu^{3+} nanoparticles also have a relatively high quantum efficiency and brightness in comparison with the other rare-earth doped nanophosphors.[3,6,7] Consequently, the luminescence properties of YVO_4:Eu^{3+} nanoparticles have aroused great interest. Among the different host materials researched, much attention has been given especially to YVO_4:Eu^{3+} also, because it can be crystallized at low temperatures to obtain much smaller nanocrystals more easily. Nevertheless, YVO_4:Eu nanoparticles have still comparably low (about 20%) quantum yield,[3,4,21] which is much lower than the quantum yield for bulk YVO_4:Eu. One of the possible reasons of low luminescence efficiency in YVO_4:Eu nanoparticles could be surface loss processes. In order to suppress them, it was suggested to apply core shell layers of YF_3 around YVO_4:Eu nanoparticles.[22] Comparison of luminescence properties for bulk, nano, and core-shelled nano YVO_4:Eu will be extremely useful for the understanding of surface loss processes, as well as it could help modify nanosized YVO_4:Eu in order to get nanopowders with high quantum yield.

Another material discussed in this paper, lanthanum phosphate ($LaPO_4$), also known as monazite, has been widely used as a phosphor and proton conductor, as well as in sensors, lasers, ceramic materials, catalysts, and heat-resistant

[a]Author to whom correspondence should be addressed. Electronic mail: vpank@latnet.lv. Fax: +371-67 132 778.

materials. This is due to its interesting properties, such as very low solubility in water, high thermal stability, high index of refraction, and so on.[23–27] Rare earth orthophosphates as host matrices—and $LaPO_4$ in particular—also exhibit quite a good ionizing and particle radiation as well as photochemical stability. This is why $LaPO_4$ has been also suggested as a prospective waste form for high-level nuclear waste.[28,29]

In recent years, $LaPO_4$ has been also shown to be a useful host lattice for lanthanide ions to produce phosphors that emit in a broad range of colors.[23,27,30–32] Even in 1963, it was already known that $LaPO_4$:0.01Ce^{3+} is a "short luminescence delay time phosphor" and emits ultraviolet (UV) light, which peaks spectrally at about 340 nm, when excited with cathode rays, and its luminescence decay time is about 24 ns.[33] Doping with different types of rare earth ions (Eu^{3+}, Ce^{3+}, Tb^{3+}, Nd^{3+}, Er^{3+}, Pr^{3+}, Ho^{3+}, Yb^{3+}, Tm^{3+}) in macro- as well as nanosized $LaPO_4$ has been frequently reported in the literature. Among all these phosphate-type phosphors, trivalent cerium (Ce^{3+}) and terbium (Tb^{3+}) co-activated $LaPO_4$ ($LaPO_4$:Ce,Tb) bulk powder is known as most efficient because of the high-efficiency energy transfer between Ce^{3+} and Tb^{3+}.[23,27,30–32] Bulk $LaPO_4$:Ce,Tb is also intensely used as an excellent green emitting phosphor for fluorescent lamps.[27,34,35] Nowadays, $LaPO_4$:Ce,Tb is known as one of the most promising highly luminescent green phosphors which is one of the best candidates for biomedical applications, such as fluorescence resonance energy transfer (FRET) assays, biolabeling, optical imaging, or phototherapy,[36–38] where green emission from Tb^{3+} is highly important. However, under UV excitation (for instance, under 254-nm radiation of mercury discharge lamps), only forbidden f-f transitions of Tb^{3+} in $LaPO_4$ could be excited and, therefore in this case, Tb^{3+} emission is not efficient. On the other hand, allowed f-d transition in a Tb^{3+} ion lays at much higher energies, i.e., at VUV spectral range. Thus, in order to effectively absorb relatively low energy UV light, a sensitizer should be used. In $LaPO_4$ phosphor, Ce^{3+} ions with effective 4f-5d absorption behave as the sensitizer, whereas Tb^{3+} ions act as the luminescent center. Indeed, under UV excitation of Ce^{3+} ion, a $4f^1 \rightarrow 4f^05d^1$ transition occurs. After energy transfer from Ce^{3+} to Tb^{3+}, a green Tb^{3+} emission resulting from $^5D_4 \rightarrow {}^7F_J$ relaxation takes place. Despite luminescence properties of bulk $LaPO_4$:Ce,Tb, as well as energy transfer processes between Ce^{3+} and Tb^{3+} ions, which have been intensively studied before,[34,39–42] we have recently suggested alternative mechanism of energy transfer via the so-called impurity trapped exciton states in nanosized $LaPO_4$:Ce,Tb[43] by analogy with some other wide bandgap materials.[44–46]

Most of the studies reported in the literature were performed using laser or ultraviolet lamps as an excitation sources, while, for instance, $LaPO_4$ belongs to the class of wideband-gap materials, and its experimental bandgap was reported to be around 8.0 eV.[47,48] To extend the excitation energy range, in this paper, we use the pulsed synchrotron radiation, which, due to its broad and continuous spectrum, is a very useful tool for the investigation of optical and luminescence properties of wideband-gap materials,[49–54] where UV and VUV excitations are dominant.

II. EXPERIMENT

A. Nanophosphors synthesis

Both types of luminescent $LaPO_4$:Ce,Tb and YVO_4:Eu nanopowders were produced via a microwave-accelerated synthesis in ionic liquids. This method was described in detail elsewhere.[22,55–57]

The crystallinity of as prepared $LaPO_4$:Ce,Tb is proven by powder x ray diffraction (PXRD) pattern[55] as well as by high-resolution transmission electron microscopy (HRTEM). Both types of method—as expected—indicate the nanoparticles to crystallize with the monazite type of structure. With the assumption of spherical particles, a mean particle diameter of 8–10 nm is calculated using Scherrer's equation. This value agrees with that determined by electron microscopy.[55] The dopant concentration of 45 mol. % Ce^{3+} and 15 mol. % Tb^{3+} is quite common for $LaPO_4$:Ce,Tb phosphors.[34] Due to the similar radii of the three-valent rare-earth ions, phase separation does not occur.[34,35] The composition and the amount of dopants are confirmed by energy-dispersive x ray analysis (EDX). Pressed pellets of the as-prepared nanopowder show values of: 39 (1) mol. % La (expected 40 mol. %), 46 (1) mol. % Ce (expected 45 mol. %), and 15 (1) mol. % Tb (expected 15 mol. %). Commercial macroscopic $LaPO_4$:Ce,Tb powder with the same dopants level was also used in the current study as a reference material in the luminescence measurements.

The details of the synthesis procedure of YVO_4:Eu nanopowders, as well as the result of the sample's characterizations by means of electron microscopy, energy loss spectroscopy, infrared spectroscopy, dynamic light scattering (DLS), and x ray diffraction analysis (XRD), have been reported in Ref. 22. According to electron microscopy, DLS, and XRD, the presence of uniform and highly crystalline particles, 12–15 in diameter, is validated. As-prepared particles turn out to be non-agglomerated and redispersible. Commercial bulk YVO_4:Eu powder (with particle size several microns) from Phillips was also characterized by means of UV-VUV luminescence spectroscopy for comparison. The dopant level in nanosized YVO_4:Eu was 15 mol. %, whereas bulk YVO_4:Eu was typically doped with 5 mol. %. In order to minimize possible surface-related losses, YVO_4:Eu nanoparticles have been covered by a nonluminescent 1-2 nm thickness YF_3 layer, as was described in Ref. 22. Such a sample is denoted in the paper as YVO_4:Eu@YF_3.

B. Luminescence characterization

In the present study, luminescence properties of nanophosphors in the UV-VUV spectral range were studied with pulsed synchrotron radiation from the DORIS III storage ring of the Deutsches Elektronen-Synchrotron DESY (Hamburg, Germany). The Superlumi experimental station of HASYLAB was used for the measurements of emission and excitation spectra.[58] The excitation spectra were recorded in the 330-30 nm (3.7-40 eV) spectral range with a spectral resolution of 0.3 nm. Excitation spectra of sodium salicylate were normalized to equal synchrotron radiation intensities impinging onto the sample. Luminescence spectra in the UV

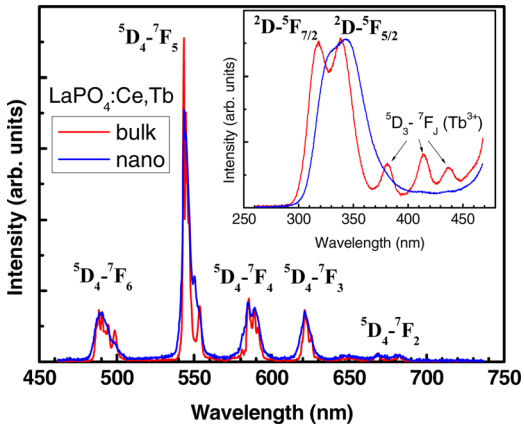

FIG. 1. (Color online) Emission spectra of Tb^{3+} and Ce^{3+} ions (inset) in the macroscopic and nanosized $LaPO_4$:Ce,Tb under excitation in the Ce^{3+} absorption band (250 nm) at 10 K.

and visible/infrared range were recorded with a monochromator (SpectraPro-308i, Acton Research Corporation) equipped with a liquid nitrogen-cooled CCD detector (Princeton Instruments) and a photomultiplier (HAMAMATSU R6358P). The spectral resolution of the analyzing monochromator was typically 11 nm. Emission spectra were corrected for the spectral response of the detection system. Powders were slightly pressed into pellets and installed onto the sample holder of a flow-type liquid helium cryostat.

It is necessary to note that both materials belong to the class of radiation-resistant oxide materials in which radiation damage occurs via particles elastic collisions only; that is not the case for 3.7-40 eV photons.[59,60]

III. RESULTS AND DISCUSSION

A. $LaPO_4$:Ce,Tb

Let us start with demonstration of distinctions in luminescence properties (especially in the VUV range) between bulk and nanosized $LaPO_4$:Ce,Tb. Emission spectra of Tb^{3+} and Ce^{3+} ions for both bulk and nanosized $LaPO_4$:Ce,Tb are demonstrated in Fig. 1. The spectra were excited by 250-nm photons, which correspond to a $4f^1 \rightarrow 4f^05d^1$ transition in the Ce^{3+} ion. From Fig. 1, it is clearly seen that a significant discrepancy between emission spectra for bulk and nano samples takes place. Detailed analysis of the emission spectra was done in Ref. 54, taking into account fine structures of both Ce^{3+} and Tb^{3+} emission bands. It was suggested there that a strong perturbation of the crystal field of rare-earth ions due to a small nanoparticle size leads to the changes in the emission spectra.

The excitation spectra for both Ce^{3+} and Tb^{3+} emissions are depicted in Figs. 2(a) and 2(b) for the bulk and the nanosized $LaPO_4$:Ce,Tb samples, respectively. The excitation spectrum of Ce^{3+} emission in the 4.0–6.5 eV range for the bulk $LaPO_4$:Ce,Tb (Fig. 2(a)) ordinates due to 4f-5d transition in Ce^{3+} ion in $LaPO_4$ matrix. This spectrum is composed of five bands peaking at 4.46 eV, 4.76 eV, 5.2 eV, 5.8 eV, and 6.05 eV, which are due to the transition from the ground state $^2F_{5/2}$ ($4f^1$) to the five crystal-field split levels of the ^2D ($5d^1$) excited state in the $LaPO_4$ lattice. These bands are similar to those observed for cerium-doped $LaPO_4$ and reported before in Ref. 61.

The low energy part of the excitation spectrum of Tb^{3+} emission, where f-f transition in Tb^{3+} occur (4.0–5.6 eV), is very close to the excitation spectrum of Ce^{3+} emission (Fig. 2(a)). Note, according to Ref. 61, such intensive excitation is practically negligible in the excitation spectrum of Tb^{3+} emission in terbium-doped $LaPO_4$. Taking into account that f-f transitions of Tb^{3+} emission are not effective in this spectral range, it is naturally concluded that the intensive excitation of Tb^{3+} emission in the 4.0–5.6 eV range appears due to energy transfer from Ce^{3+} to Tb^{3+}. On the other hand, f-d transitions in Tb^{3+} ions become dominant at energies higher than 5.6 eV and, therefore, Tb^{3+} emission can be excited directly, i.e., without energy transfer via Ce^{3+} states. A crystal-field splitting is responsible for a prodigious structure of the Tb^{3+} excitation spectrum at energies higher than 5.6 eV (Fig. 2(a)). In this case, the transitions from the ground state ^7F ($4f^8$) to the lowest ^7D ($4f^75d$) and to the lowest ^9D ($4f^75d$) term leads to formation of ten bands in the Tb^{3+} excitation spectrum (Fig. 2(a)) in the 5.6–7.7 eV range. These bands are described in detail in Ref. 12 for terbium-doped bulk $LaPO_4$.

The excitation spectrum for Ce^{3+} emission in nanosized $LaPO_4$:Ce,Tb has intensive bands in the 3.5–6.5 eV spectral range (Fig. 2(b)), which are qualitatively similar to the corresponding excitation obtained for bulk $LaPO_4$:Ce,Tb in Fig.

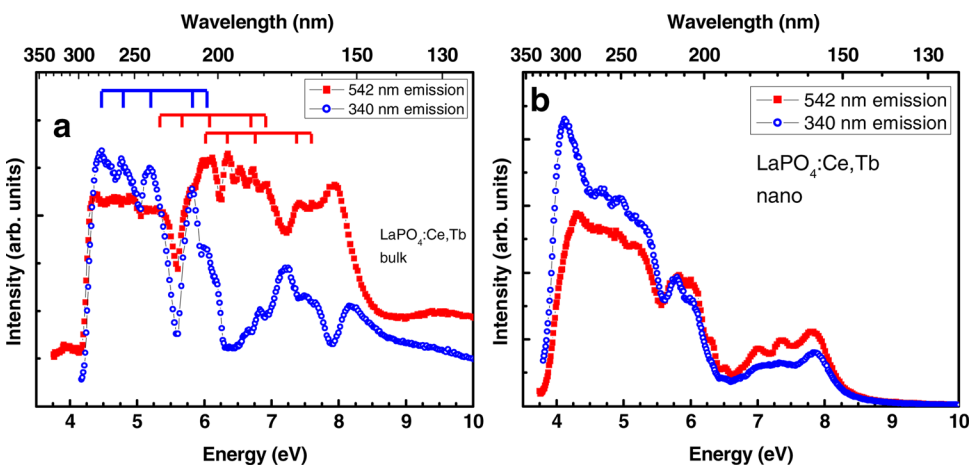

FIG. 2. (Color online) Excitation spectra of Ce^{3+} (340 nm) and Tb^{3+} (542 nm) emissions in the macroscopic (a) and nanosized (b) $LaPO_4$:Ce,Tb at 10 K. The positions of crystal-field split Ce^{3+} and Tb^{3+} bands in $LaPO_4$:Ce and $LaPO_4$:Tb obtained in Ref. 61 are demonstrated by red and blue scale lines for comparison.

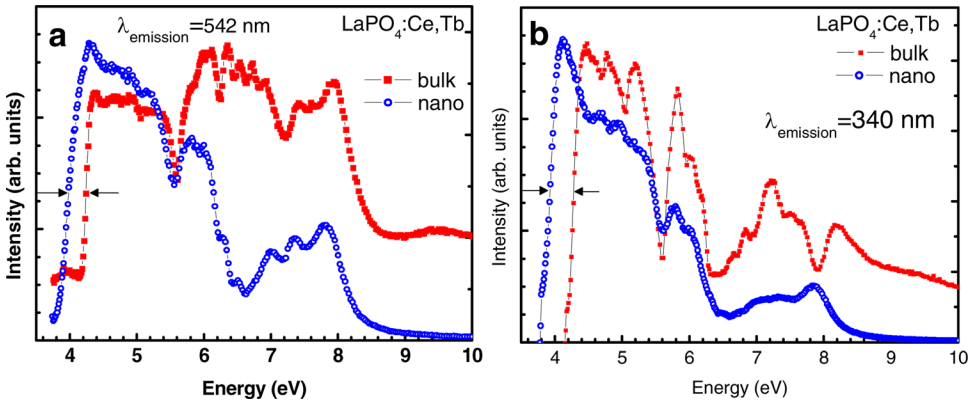

FIG. 3. (Color online) Comparison of excitation spectra of Tb^{3+} (542 nm) (a) and Ce^{3+} (340 nm) (b) emissions for bulk and nanosized $LaPO_4$:Ce,Tb at 10 K in 3.5–10 eV spectral range.

2(a). On the other hand, the excitation spectrum of Tb^{3+} emission in the nano sample is drastically changed compared with the bulk one. Indeed, the part of the excitation spectrum due to f-d transitions in the Tb^{3+} ion (5.6 eV and higher) is significantly suppressed in nano $LaPO_4$:Ce,Tb. This result is in contradiction to the Tb^{3+} excitation spectrum in the bulk sample, where significant contribution of f-d transition in Tb^{3+} was detected in the 5.6–7.7 eV range (Fig. 2(a)). It means that Tb^{3+} ions practically cannot be directly excited in nanosized $LaPO_4$:Ce,Tb, but could be excited after energy transfer from Ce^{3+} only. We suggest that, due to small nanoparticle size and high impurity concentration, Tb^{3+} and Ce^{3+} ions are closely distributed, i.e., no isolated Tb^{3+} ions in nanoparticles. Since a cerium concentration is three times higher than a terbium one, Ce^{3+} ions "shield" Tb^{3+} ions, and Ce^{3+} ions' excitation is very probable.

In fact, the distinctions in the excitation spectra between bulk and nano samples for both Ce^{3+} and Tb^{3+} emissions are especially well demonstrated in Fig. 3 and Fig. 4. First of all, it is evident that, exploring the low energy part of the excitation spectra, a redshift is detected in the excitation spectra for the nano sample (pointed by arrows on Fig. 3). This redshift looks the same for both Ce^{3+} and Tb^{3+} emissions. As we already mentioned above, Tb^{3+} emissions are excited via Ce^{3+} states at energies below 5.6 eV. Therefore, it is natural that the excitation spectrum of Tb^{3+} has similar peculiarities comparing with the excitation spectrum of Ce^{3+} emission in this spectral range. It is supposed that the redshift of the excitation spectra is due to perturbation of 5d levels of Ce^{3+} ions in nanosized $LaPO_4$:Ce,Tb. As a result of such perturbation, the 5d excited state is slightly shifted and Ce^{3+} excitation spectrum in nano $LaPO_4$:Ce,Tb is shifted to the low energy side, comparing with the corresponding spectrum for the bulk sample.

Other significant differences between the excitation spectra for bulk and nano $LaPO_4$ (Fig. 3) are clearly revealed in the 6.5-8.5 eV spectral range. Taking into account bandgap energy of $LaPO_4$ (8 eV), the excitation bands in this spectral range could belong to excitonic excitation bands (including self-trapped and/or bound excitons). Optical properties of excitons are extremely sensitive to nanoparticle size, due to the increasing role of surface effects. Thus, the changes in the excitation spectra in the 6.5-8.5 eV spectral range could be induced by the nanoparticle's surface on the excitons in nanosized $LaPO_4$. For instance, the excitation bands of the bound exciton near Ce^{3+} are well resolved in the 6.5-8.0 eV range in bulk $LaPO_4$:Ce,Tb, whereas these bands are significantly smoothed and suppressed in the nanopowder (Fig. 3(b)), obviously due to surface influence.

Important information could be retrieved from Fig. 4 examining the excitation spectra at energies higher than 8 eV. In contrast to the bulk material, both Ce^{3+} and Tb^{3+} emissions practically could not be excited in the nanopowders if the excitation energy exceeds the bandgap energy of

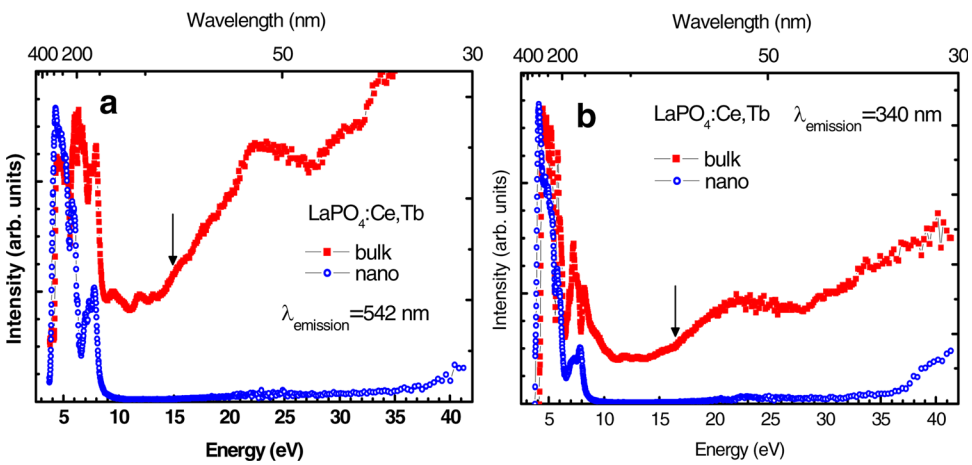

FIG. 4. (Color online) Comparison of excitation spectra of Tb^{3+} (542 nm) (a) and Ce^{3+} (340 nm) (b) emissions for bulk and nanosized $LaPO_4$:Ce,Tb at 10 K in wide spectral range (3.5–40 eV). Black arrows point out the initial stage of MEE processes.

$LaPO_4$. This fact clearly indicates that there is no energy transfer from the $LaPO_4$ matrix to the Ce^{3+} and Tb^{3+} ions in nanoparticles. Processes occurring under high energy excitations could be briefly considered as follows: After high energy excitations (higher than 8 eV), electrons in the conduction band and holes in the valence band are created. In the bulk sample, after some relaxations, electrons and holes are trapped by dopants, forming excited Ce^{3+} and Tb^{3+} ions, and their radiative relaxation leads to Ce^{3+} and Tb^{3+} emissions. On the other hand, electrons and holes in the nanoparticles could be easily trapped by surface defects, where their non-radiative relaxation occurs. Such process is a competing relaxation channel, comparing with the radiative relaxation (luminescence), and it should be very efficient in nanoparticles, where the role of surface states is dominated. Therefore, it is suggested that electrons and holes effectively trapped by the nanoparticle's surface and such surface-related loss processes are a main reason of luminescence vanishing under high energy excitations in nanosized $LaPO_4$:Ce,Tb. Negligible luminescence intensity of nanosized $LaPO_4$:Ce,Tb under high energy excitation definitely restricts these materials' utilization in some practical applications, for instance, as so-called "slow scintillators" for security applications.

The shape of the excitation spectra in the bulk $LaPO_4$ sample could depend on many different processes and parameters, which are considered in detail elsewhere. One of the most interesting processes occurring under high energy excitations is so-called multiplication of electronic excitations (MEE). MEE processes' creation means that two or more luminescence centers are created per one absorbed photon. For a successful realization of MEE processes, the excitation energy of the photon must exceed a threshold energy $E_{th} = 2E_g$, where E_g is the bandgap energy. MEE processes in wide bandgap materials were studied in detail in Refs. 62 and 63; however, such processes could be also successfully realized in semiconductor nanocrystals.[64,65] It is clearly seen from Fig. 4 that, for bulk $LaPO_4$:Ce,Tb, the rise of the excitation intensity for both Ce^{3+} and Tb^{3+} emissions starts at about 15-17 eV. This value is very close to the value of $2E_g$, keeping in mind that E_g in $LaPO_4$ is 8 eV.

B. YVO_4:Eu

Emission spectra for bulk and two nano (as-grown and YF_3-covered) YVO_4:Eu samples reveal the characteristic Eu^{3+} emission lines (Fig. 5), which are well known in the literature.[3,4,22,66] In contrast to the $LaPO_4$:Ce,Tb phosphor considered above in Subsection III A, the bandgap of YVO_4 is comparably small ($E_g \approx 3.4$ eV). It means that, even under comparably low 300-nm excitation, europium luminescence could be excited only after energy transfer from the YVO_4 matrix to Eu^{3+} ions with subsequent f-f radiative relaxation ($^5D_0 \rightarrow {}^7F_J$ transitions). Therefore, Eu^{3+} emission should be very sensitive to surface-related losses in YVO_4 nanoparticles. Surface-related losses mean that electronic excitations are captured by surface defects and/or imperfections with subsequent non-radiative annihilation. Under band-to-band excitation, electrons and holes form an excited intrinsic molecular complex $(VO_4)^{3-}$. The energy transfer from the $(VO_4)^{3-}$ complex to the activator ion leads to Eu^{3+} emission. However, electrons and holes could be also trapped on the surface instead of the formation of the $(VO_4)^{3-}$ complex. Therefore, surface-related loss could be considered as one of the competing relaxation channels under band-to-band excitation in nanoparticles.

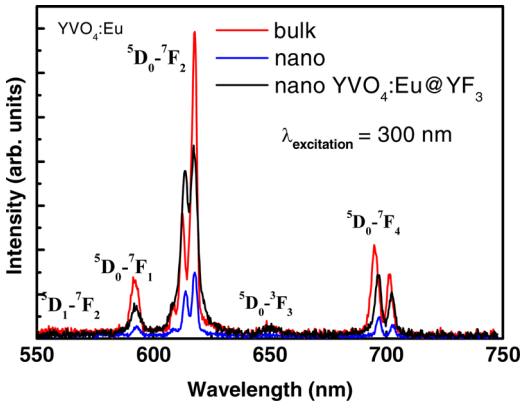

FIG. 5. (Color online) Emission spectra of Eu^{3+} ions in the macroscopic, nanosized, and nanosized YF_3-covered YVO_4:Eu at 10 K.

We did not compare quantum yields for three samples; however, special experiment conditions were provided for in order to compare intensities of luminescence for these three samples. It is clear (Fig. 5) that luminescence intensity drops down in the nanopowder, comparing with the bulk material. On the other hand, after surface passivation by the core shell layer, luminescence intensity could by significantly increased.

It is interesting to note that, in contrast to the emission spectra of $LaPO_4$:Ce,Tb depicted in Fig. 1, the fine structure of Eu^{3+} emission bands is well resolved even in YVO_4:Eu nanocrystals. It could mean that crystal field symmetry around Eu^{3+} ions does not suffer from the nanoparticle's surface.

The excitation spectra for Eu^{3+} emission in the three samples studied are depicted in Fig. 6–the low energy part is shown in detail in Fig. 6(a), whereas the whole spectra are demonstrated in Fig. 6(b). These spectra are normalized for better comparison. At least three peaks could be resolved in the excitation spectra for all samples studied: at 4 eV, 5 eV, and 6 eV (Fig. 6(a)). Similar peaks were observed before for bulk YVO_4:Eu in Ref. 67 (dashed line in Fig. 6(a)). Taking into account that similar excitation spectra are observed for YVO_4:Eu samples, which were produced by different methods, we can conclude that the structure of the excitation spectra in the 3.5–7.0 eV spectral range has intrinsic nature. For instance, we suppose that the density of states of vanadate bands is responsible for the structure of the excitation spectra.

The most significant distinction in the excitation spectra between bulk and nano YVO_4:Eu is observed in the high energy part (Fig. 6(b)). The excitation spectrum for bulk YVO_4:Eu has a strong rise at energies higher than 10 eV, reaching maximum at 30 eV. It is necessary to note that the intensity of the excitation peak at 30 eV is very close to the most intensive peak at 4 eV. Such strong intensive excitation

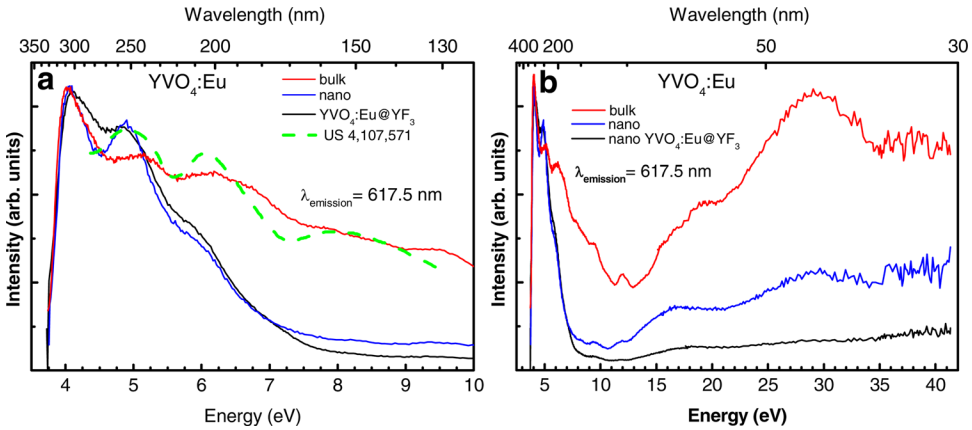

FIG. 6. (Color online) Excitation spectra of Eu^{3+} (617.5 nm) emission in the bulk, nanosized, and nanosized YF_3-covered YVO_4:Eu at 10 K in 3.5–10 eV (a) and 3.0–40 eV (b) spectral ranges. The excitation spectrum of Eu^{3+} taken from Ref. 67 (dashed line) is given in (a) for comparison.

of Eu^{3+} emission with photons with energies near 25 eV could have a practical application, for instance, in helium discharge lamps, taking into account the first ionization potential 24.581 eV of helium gas. Unfortunately, the origin of the intensive excitation in the 10–40 eV range in bulk YVO_4:Eu is unclear so far, and further investigation is required.

Exploring the excitation spectra for nanosized YVO_4:Eu and nanosized core shell-covered YVO_4:Eu, we can conclude that MEE processes are strongly suppressed there. Indeed, intensity of the excitation peak at 30 eV in nanosized YVO_4:Eu is about 30%, but in nanosized YVO_4:Eu@YF, it is about 10%, comparing with the bulk sample. The degradation of the excitation spectrum in nano YVO_4:Eu could be explained by an analogy with $LaPO_4$:Ce,Tb, considered above, i.e., by charge carriers trapping by surface defects with subsequent non-radiative relaxation. On the other hand, it is surprising that surface passivation by the nanoparticle covering in the YVO_4:Eu@YF sample does not increase the intensity of the excitation peak in the 10–45 eV range. Moreover, the intensity of this peak even decreases. It was expected that surface covering should passivate the surface defects, which are responsible for surface losses' processes, but in reality, we got the opposite result. It is necessary to note that the main difference between excitation spectra for nano YVO_4:Eu and YVO_4:Eu@YF_3 samples starts at energies higher than 10 eV (Fig. 6(b)) Taking into account that the bandgap energy of YF_3 is about 11 eV,[51] it is supposed that the YF_3 layer around the YVO_4:Eu nanoparticles works as a "shield", partially absorbing the excitation energy intended for the YVO_4:Eu core.

IV. CONCLUSION

Detailed investigation of luminescence properties of nano and macro-sized $LaPO_4$:Ce,Tb and YVO_4:Eu phosphors has been done in a wide spectral range, including the vacuum ultraviolet spectral range. It was demonstrated that nanoparticles' surface can drastically change emission and excitation spectra of nanopowders, comparing with corresponding bulk materials. Especially significant distinctions between excitation spectra for nano and bulk materials were observed under relatively high energy excitation (exceeding 10 eV). It was suggested that surface-related loss processes, namely electron-hole pairs' non-radiative annihilation at the surface, are responsible for the suppression of energy transfer processes from the host lattice to impurity ions and, subsequently, for rare-earth emission degradation under high energy excitations in nanosized materials.

ACKNOWLEDGMENTS

The experiments at DESY leading to these results have received funding from the European Community's Seventh Framework Programme (FP7/2007-2013) under grant agreement No. 226716. The work of V. Pankratov and L. Shirmane was granted by ESF Project No. 2009/0202/1DP/1.1.1.2.0/09/APIA/VIAA/141. The research of A.I. Popov was partially supported by Sadarbības projekts No. 10.0032.

[1]A. K. Levine and F.C. Palilla, Appl. Phys. Lett. **5**, 118 (1964).
[2]A. Bril, W. L. Wanmaker, and J. Broos, J. Chem. Phys. **43**, 311 (1965).
[3]K. Riwotzki and M. Haase, J. Phys. Chem. B **102**, 10129 (1998).
[4]K. Riwotzki and M. Haase, J. Phys. Chem. B **105**, 12709 (2001).
[5]T. Minami, T. Miyata, Y. Suzuki, and Y. Mochizuki, Thin Solid Films **65**, 469 (2004).
[6]A. Huignard, T. Gacoin, and J. Boilot, Chem. Mater. **12**, 1090 (2000).
[7]A. Huignard, V. Buissette, A. Franville, T. Gacoin, and J. Boilot, J. Phys. Chem. B **107**, 6754 (2003).
[8]M. Yu, J. Lin, Z. Wang, J. Fu, S. Wang, H. J. Zhang, and Y. C. Han, Chem. Mater. **14**, 2224 (2002).
[9]F. M. Nirwan, T. K. Gundu Rao, P. K. Gupta, and R. B. Pode, Phys. Status Solidi A **198**, 447 (2003).
[10]D. K. Williams, B. Bihari, and B. M. Tissue, J. Phys. Chem. B **102**, 916 (1998).
[11]H. Zhang, M. Lü, Z. L. Xiu, G. J. Zhou, S. F. Wang, Y. Y. Zhou, and S. M. Wang, Mater. Sci. Eng. B **130**, 151 (2006).
[12]Y. J. Sun, H. J. Liu, X. Wang, X. G. Kong, and H. Zhang, Chem. Mater. **18**, 2726 (2006).
[13]L. M. Chen, Y. N. Liu, and K. L. Huang, Mater. Res. Bull. **41**, 158 (2006).
[14]P. Ghosh, A. Kar, and A. Patra, J. Appl. Phys. **108**, 113506 (2010).
[15]L. R. Singh and R. S. Ningthoujam, J. Appl. Phys. **107**, 104304 (2010).
[16]S. Okamoto, R. Uchino, K. Kobayashi, and H. Yamamoto, J. Appl. Phys. **106**, 013522 (2009).
[17]K. S. Shim, H. K. Yang, Y. R. Jeong, B. K. Moon, B. C. Choi, J. H. Jeong, J. S. Bae, S. S. Yi, and J. H. Kim, Appl. Surf. Sci. **253**, 8146 (2007).
[18]C. Breacher, H. Samelson, A. Lempicki, R. Riley, and T. Peters, Phys. Rev. **155**, 178 (1967).
[19]E. D. Reed and H. W. Moos, Phys. Rev. B **8**, 980 (1973).
[20]E. D. Reed and H. W. Moos, Phys. Rev. B **8**, 988 (1973).
[21]A. Huignard, T. Gacoin, and J. P. Boillot, Chem. Mater. **12**, 1090 (2000).
[22]A. Zharkouskay, H. Lünsdorf, and C. Feldmann, J. Mater. Sci. **44**, 3936 (2009).

[23]N. Hashimoto, Y. Takada, K. Sato, and S. Ibuki, J. Lumin. 48-49, 893 (1991).
[24]T. Norby and N. Christiansen, Solid State Ionics **77**, 240 (1995).
[25]Y. Hikichi, T. Ota, K. Daimon, T. Hattori, and M. Mizuno, J. Am. Ceram. Soc. **81**, 2216 (1998).
[26]Y. Fang, A. Xu, R. Song, H. Zhang, L. You, J. C. Yu, and H. Liu, J. Am. Chem. Soc. **125**, 16025 (2003).
[27]C. Feldmann, T. Jüstel, C. R. Ronda, and P. J. Schmidt, Adv. Funct. Mater. **13**, 511 (2003).
[28]G. J. McCarthy, W. B. White, and D. E. Pfoertsch. Mater. Res. Bull. **13**, 1239 (1978).
[29]A. Meldrum, L. A. Boatner, and R. C. Ewing, Phys. Rev. B **56**, 13805 (1997).
[30]K. Riwotzki, H. Meyssamy, H. Schnablegger, A. Kornowski, and M. Haase, Angew. Chem., Int. Ed. **40**, 573 (2001).
[31]S. Heer, O. Lehmann, M. Haase, and H. U. Güdel, Angew. Chem., Int. Ed. **42**, 3179 (2003).
[32]K. Riwotzki, H. Meyssamy, A. Kornowski, and M. Haase, J. Phys. Chem. B **104**, 2824 (2000).
[33]C. W. Struck, Short luminescence delay time phosphors, U.S. patent 3,104,2246 (1963).
[34]G. Blasse and B. C. Grabmaier, Luminescent Materials (Springer-Verlag, Berlin, 1994).
[35]Phosphor Handbook, edited by W. M. Yen and S. Shionoya (CRC Press, Boca Raton, FL, 1999).
[36]B. Dubertret, P. Skourides, D. J. Norris, V. Noireaux, A. H. Brivanloue, and A. Libchaber, Science **298**, 1759 (2002).
[37]T. Pellegrino, S. Kuders, T. Liedl, A. M. Javier, L. Manna, and W. Parak, Small **1**, 48 (2005).
[38]C. R. Patra, R. Bhattacharya, S. Patra, S. Basu, P. Mukherjee, and D. Mokhopadhyay, J. Nanobiotechnol. **4**, 11 (2006).
[39]W. van Schaik, S. Lizzo, W. Smit, and G. Blasse, J. Electrochem. Soc. **140**, 216 (1993).
[40]J. M. P. J. Verstegen, J. L. Sommerdijk, and J. G. Verriet, J. Lumin. **6**, 425 (1973).
[41]J.-C. Bourcet and F. K. Fonf, J. Chem. Phys. **60**, 34 (1973).
[42]Ph. Meunier-Beillard, B. Moine, C. Dujardin, X. Cieren, C. Pedrini, D. Huguenin, and V. Archambault, Radiat. Eff. Defects Solids **149**, 25 (1999).
[43]V. Pankratov, A. I. Popov, S. A. Chernov, A. Zharkouskaya, and C. Feldmann, Phys. Status Solidi B **247**, 2252 (2010).
[44]D. S. McClure and C. Pedrini, Phys. Rev. B **32**, 8465 (1985).
[45]B. Moine, C. Pedrini, and V. Ghiordanescu, J. Phys.: Condens. Matter **6**, 4093 (1994).
[46]S. A. Chernov, L. Trinkler, and A. I. Popov, Radiat. Eff. Defects Solids **143**, 345 (1998).
[47]E. Nakazawa and F. Shiga, J. Lumin. **15**, 255 (1977).
[48]U. Sasum, M. Kloss, A. Rohmann, L. Schwarz, and D. Haberland, J. Lumin. **72-74**, 255 (1997).
[49]H. H. Rüter, H. V. Seggern, R. Reininger, and V. Saile, Phys. Rev. Lett. **65**, 2438 (1990).
[50]M. Kirm, G. Zimmerer, E. Feldbach, A. Lushchik, Ch. Lushchik, and F. Savikhin, Phys. Rev. B **60**, 502 (1999).
[51]V. Pankratov, M. Kirm, and H. von Seggern, J. Lumin. **113**, 143 (2005).
[52]V. Pankratov, L. Grigorjeva, S. Chernov, T. Chudoba, and W. Lojkowski, IEEE Trans. Nucl. Sci. **55**, 1509 (2008).
[53]A. Kalinko, A. Kotlov, A. Kuzmin, V. Pankratov, A. I. Popov, and L. Shirmane, Cent. Eur. J. Phys. **9**, 432 (2011).
[54]V. Pankratov, A. I. Popov, A. Kotlov, and C. Feldmann, Opt. Mater. **33**, 1102 (2011).
[55]G. Bühler and C. Feldmann, Angew. Chem., Int. Ed. **45**, 4864 (2006).
[56]G. Bühler and C. Feldmann, Appl. Phys. A **87**, 631 (2007).
[57]A. Zharkouskaya, C. Feldmann, K. Trampert, W. Heering, and U. Lemmer, Eur. J. Inorg. Chem. 873 (2008).
[58]G. Zimmerer, Radiat. Meas. **42**, 859 (2007).
[59]E. A. Kotomin and A. I. Popov, Nucl. Instrum. Methods Phys. Res. B **141**, 1 (1998).
[60]A. I. Popov, E. A. Kotomin, and J. Maier, Nucl. Instrum. Methods Phys. Res. B **268**, 3084 (2010).
[61]E. Nakazawa and F. Shiga, Jpn. J. Appl. Phys. **42**, 1642 (2003).
[62]M. Kirm, I. Martinson, A. Lushchik, K. Kalder, R. Kink, Ch. Lushchik, and A. Löhmus, Solid State Commun. **90**, 741 (1994).
[63]A. Lushchik, A. M. Kirm, Ch. Lushchik, I. Martinson, V. Nagirnyi, F. Savikhin, and E. Vasil'chenko, Nucl. Instrum. Methods Phys. Res. A **537**, 45 (2005).
[64]V. Pankratov, V. Osinniy, A. Kotlov, A. Nylandsted Larsen, and B. Bech Nielsen, Phys. Rev. B **83**, 045308 (2011).
[65]M. C. Beard, K. P. Knutsen, P. Yu, J. M. Luther, Q. Song, W. K. Metzger, R. J. Ellingson, and A. J. Nozik, Nano Lett. **7**, 2506 (2007).
[66]M. Haase, K. Riwotzki, H. Meyssamy, and A. Kornowski, J. Alloys Compd. **191**, 303 (2000).
[67]S. Tanimizu, T. Suzuki, and T. Fukuzawa, Light emitting device having luminescent screen with self activated blue light emitting phosphor, U.S. patent 4,107,571 (1978).

Physica B 504 (2017) 80–85

Contents lists available at ScienceDirect

Physica B

journal homepage: www.elsevier.com/locate/physb

Comparing the luminescence processes of YVO_4:Eu and core-shell YVO_4@YF_3 nanocrystals with bulk-YVO_4:Eu

L. Shirmane[a,*], C. Feldmann[b], V. Pankratov[a,c,d,**]

[a] Institute of Solid State Physics, University of Latvia, 8 Kengaraga iela, LV-1063 Riga, Latvia
[b] Institute of Inorganic Chemistry, Karlsruhe Institute of Technology (KIT), Engesserstrasse 15, D-76131 Karlsruhe, Germany
[c] MAX IV Laboratory, Box 118, S-221 00 Lund, Sweden
[d] Research Center of Molecular Materials, University of Oulu, P.O. Box 3000, FIN-90014 Oulu, Finland

ARTICLE INFO

Keywords:
YVO_4:Eu^{3+}
Nanophosphors
Core-Shelled nanoparticles
Luminescence
Synchrotron radiation

ABSTRACT

Comparative analysis of bulk, non-coated and core-shelled nanocrystalline YVO_4:Eu was performed by means of time-resolved luminescence and VUV excitation luminescence spectroscopy techniques. Nanocrystalline YVO_4:Eu samples – both as-prepared and YF_3 core-shelled – have been synthesized by means of a microwave-assisted synthesis in ionic liquids, which allows to obtain 10–12 nm nanoparticles with high crystallinity. The results show noticeable differences between bulk and nanocrystalline YVO_4:Eu in photoluminescence experimental data, which explains by influence of the nanocrystal surface. A YF_3 core-shell layer around YVO_4:Eu nanoparticles partially recovers the intensity of the Eu^{3+} emission. It is demonstrated that the Eu^{3+} luminescence recovery is achieved at the expense of the suppression of the intrinsic emission but not due to the passivation of surface loss centers in core-shelled nanocrystals. It is also shown that surface loss processes are the reason of the degradation of energy transfer efficiency from the host lattice to Eu^{3+} under high-energy excitations in vacuum ultraviolet spectral range.

1. Introduction

Europium doped yttrium vanadate (YVO_4:Eu), developed in 1964 by Levine and Palilla [1], is one of the most important red phosphor materials that is known for a variety of applications in luminescence and displays, such as in cathode ray tubes, fluorescent lamps and plasma displays [2]. Since YVO_4:Eu is characterized by high energy-conversion efficiency, brightness, color purity, inherent sturdiness and excellent thermal stability, it is a promising material for the production of optical devices. Luminescence and optical properties of YVO_4:Eu^{3+} single crystals and macroscopic powders have been intensively studied for more than 30 years [1,3–8]. The absorption spectrum of YVO_4 shows a strong band in the ultraviolet (UV) region. The absorption transition stems from a charge transfer from oxygen 2p to the vanadium 3d states, creating an excited $(VO_4)^{3-}$ molecular complex. Relatively small Stokes shift of the intrinsic emission of the $(VO_4)^{3-}$ vanadate group creates favorable conditions for thermally activated energy migration. Therefore, bulk YVO_4:Eu^{3+} exhibits strong Eu^{3+} red emission because of an efficient energy transfer from the excited vanadate group to the Eu^{3+} ion. The quantum yield of bulk YVO_4:Eu is reported up to 70%, providing the bulk YVO_4:Eu^{3+} material as one of the most important red phosphor compounds [9].

In recent years synthesis and characterization of YVO_4:Eu nanocrystals have been intensively studied [10–26]. Nanocrystalline YVO_4:Eu is relevant for all applications as bulk material, in addition, thin-film application is another relevant type of application. The integration of inorganic nanoparticles into polymer thin-films has been used for the functionalization of polymer materials in marking, signaling and labeling applications [27,28]. However, the most significant application in biological labeling [29] and medicine [30] is restricted for YVO_4 due to its proven toxicity.

Several investigations are devoted to wet chemistry synthesis techniques of rare earth doped YVO_4 nanocrystals, such as sol-gel processes [20–22,31,32], solution combustion synthesis [16,33], microemulsions [34], co-precipitation reactions [35], and solvothermal methods [36]. Huignard et al. described an optimized synthesis of colloidal well-dispersed YVO_4:Eu nanocrystals through direct precipitation from Y^{3+} and VO_4^{3-} salt in water, using citrate complexing agents to limit the particles size up to 8 nm and to increase their stability [11,37]. Recently new strategies of aqueous synthesis of crystalline YVO_4:Eu nanoparticles were reported, for instance, a method based on a rigorous control of the pH and of the nucleation step via microwave

* Correspondig author at: Institute of Solid State Physics, University of Latvia, 8 Kengaraga iela, LV-1063 Riga, Latvia.
** Correspondig author at: Max IV Laboratory, Lund University, Box 118, S-221 00 Lund, Sweden.
E-mail addresses: liana.shirmane@gmail.com (L. Shirmane), vladimirs.pankratovs@oulu.fi, vpank@latnet.lvvladimirs.pankratovs@maxiv.se (V. Pankratov).

http://dx.doi.org/10.1016/j.physb.2016.10.007
Received 5 September 2016; Received in revised form 5 October 2016; Accepted 6 October 2016
Available online 07 October 2016
0921-4526/

heating, and allow a precise control of composition, nanostructure, and surface states of the luminescent nanoparticles [38]. In the current study YVO_4:Eu nanoparticles have been prepared by means of a microwave-assisted synthesis in ionic liquids, which allows to produce 10–12 nm luminescent nanoparticles with high crystallinity [39].

Despite of huge progress in YVO_4:Eu nanoparticles' synthesis, still one of the most significant drawbacks of nanocrystalline YVO_4:Eu is its comparably low (up to 20%) quantum yield [10,11], which is much lower than the quantum yield of bulk material. One of the possible reasons of low luminescence efficiency in YVO_4:Eu nanoparticles are surface loss processes, which could be partially suppressed by surface passivation. For instance, recently it was demonstrated that core shell layers around YVO_4:Eu nanoparticles can significantly improve their luminescence efficiency [23,25,40].

In this paper, we present a comparative study for bulk, nanosized and YF_3 core-shelled europium doped YVO_4 by means of photoluminescence analysis (both steady state and time-resolved) in wide spectral range including vacuum ultraviolet spectral range. The main goal of this study is to clarify the role of surface states influencing the luminescence as well as vibration properties and to obtain information about non-radiative relaxation channels in nanocrystalline YVO_4:Eu.

2. Experiment

2.1. Nanophosphors synthesis

YVO_4:Eu nanopowders were produced via a microwave-accelerated synthesis in ionic liquids. The details of synthesis procedure of YVO_4:Eu nanopowders as well as the result of sample characterization by means of electron microscopy, energy loss spectroscopy, infrared spectroscopy, dynamic light scattering (DLS), and X-ray diffraction analysis (XRD) have been reported in [40]. According to electron microscopy, DLS and XRD, the presence of uniform and highly crystalline particles, 12–15 in diameter is validated. The as-prepared nanoparticles turn out to be non-agglomerated and redispersible. The dopant level in nanosized YVO_4:Eu was 15 mol-%, whereas bulk YVO_4:Eu is typically doped with 5 mol%. In order to minimize possible surface related losses YVO_4:Eu nanoparticles have been covered by a non luminescent YF_3 layer, 1–2 nm thickness, as it was described in [40]. Such sample is denoted in the paper as YVO_4:Eu@YF_3.

Commercial bulk-YVO_4:Eu powder (with particle size of several microns) provided by Phillips was also characterized by means of luminescence spectroscopy for comparison.

2.2. Luminescence characterization

2.2.1. Time-resolved experiments

Comparative analysis of time-resolved luminescence properties under excitation of wavelength tunable pulsed solid-state laser PG401/SH pumped by PL2143/Pre-T (pulse duration ~30 ps) from Ekspla was performed. Luminescence decay kinetics were measured by Bruker Optics SPEC 250IS/SM monochromator/spectrometer coupled to a Streak Scope C4334 (time resolution better than 30 ps) from Hamamatsu. For temperature measurements from 25 to 300 K the samples have been placed into closed cycle He cryostat DE202N from Advanced Research Systems. LakeShore 325 temperature controller (accuracy ± 1 K) has been applied to control the temperature of the samples. To record luminescence spectra 266 nm excitation wavelength was used.

2.2.2. Synchrotron radiation based experiments

Utilizing synchrotron radiation for luminescence studies in UV and VUV spectral range have been successfully applied for many types of inorganic solids: wide band gap fluorides [41,42], chlorides [43], bromides [44], iodides [45], complex oxides [46–48] and even nanocrystalline semiconductor structures [49], and two-dimensional systems [50].

Luminescence properties of YVO_4:Eu nanophosphors in the current study have been studied utilizing two synchrotron radiation facilities. In the DORIS III storage ring of the Deutsches Elektronen-Synchrotron DESY (Hamburg, Germany) synchrotron radiation from *bend magnet* was utilized, whereas *undulator* I3 beamline of MAX III storage ring of MAX IV (Lund, Sweden) was applied. Both facilities were used for the measurements of emission and excitation spectra of materials in question. In the Superlumi beamline [51] of DORIS III (Photon Science, DESY) the excitation spectra were recorded in the 330–30 nm (3.7–40 eV) spectral range with a spectral resolution of 0.3 nm. Luminescence spectra in the UV and visible/infrared range were recorded with a monochromator (SpectraPro-308i, Acton Research Corporation) equipped with a liquid nitrogen cooled CCD detector (Princeton Instruments) and a photomultiplier (HAMAMATSU R6358P). The spectral resolution of the analyzing monochromator was typically 11 nm. The same registration equipment was utilized on the mobile luminescence endstation [42] installed on the FinEst branch of the I3 beamline [52,53] of MAX III ring (MAX IV-Lab). Excitation spectra of sodium salicylate were normalized to equal synchrotron radiation intensities impinging onto the sample. Emission spectra were corrected for the spectral response of the detection system. Powdered samples were slightly pressed into pellets and installed onto the sample holder of a flow-type liquid helium cryostat allowing a temperature manipulation from 10 to 350 K.

3. Results and discussion

3.1. Emission spectra

Emission spectra of bulk and the two nanocrystalline (as-prepared and YF_3-shelled) YVO_4:Eu samples are shown in Fig. 1. They reveal the characteristic Eu^{3+} emission lines (Fig. 1), which are well known in literature [10,12]. These spectra are identical under any excitation in the 3.7–40 eV energy range observed on both synchrotron based endstations. One can see that the luminescence intensity of Eu^{3+} drops down for the nanocrystalline sample in comparison to the the bulk material. On the other hand, after surface passivation by YF_3 core-shell layer, luminescence intensity significantly recovered.

Since the band gap of YVO_4 is about $E_g \approx 3.8$ eV [54] even under comparably low energy UV excitation, the Eu^{3+} luminescence could be excited only after energy transfer from the YVO_4 lattice to the Eu^{3+} ions with subsequent f-f radiative relaxation ($^5D_0 \rightarrow {}^7F_J$ transitions). Therefore, Eu^{3+} emission should be very sensitive to surface related losses of the YVO_4 nanoparticles. Surface related losses mean that electronic excitations are trapped by surface defects and/or imperfections with subsequent non-radiative annihilation. Under band-to-band

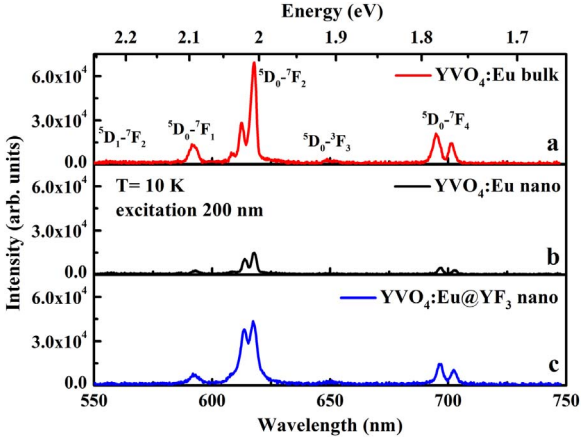

Fig. 1. High resolution luminescence spectra of Eu^{3+} in bulk, nano and core-shell layered nano YVO_4:Eu under UV excitation at 10 K.

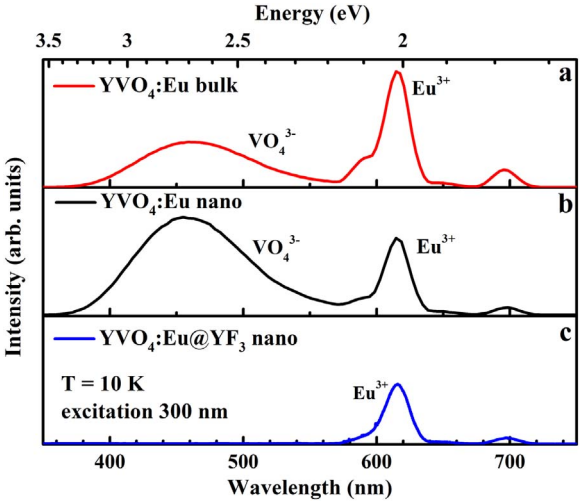

Fig. 2. Luminescence spectra of intrinsic emission in bulk, nano and core-shelled nano YVO_4:Eu under UV excitation at 10 K. Emission lines of Eu^{3+} are measured with low spectral resolution. (For interpretation of the references to color in this figure, the reader is referred to the web version of this article.)

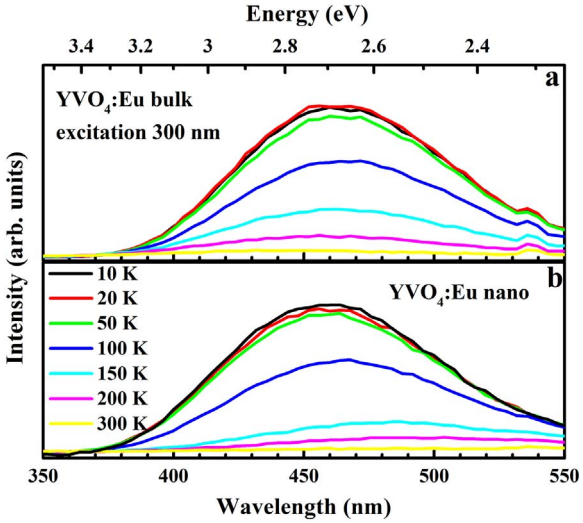

Fig. 3. Temperature dependencies of the intrinsic emission bands in bulk (a) and nanocrystalline (b) YVO_4:Eu under UV excitation.

excitation the excited intrinsic molecular complex $(VO_4^{3-})^*$ is created. The energy transfer from the $(VO_4^{3-})^*$ complex to an activator ion resulting in characteristic Eu^{3+} emission. However, electrons and holes during their thermalization could be efficiently trapped by surface loss centers instead of forming an excited $(VO_4^{3-})^*$ complex with subsequent energy transfer to Eu^{3+} ions. Therefore, non-radiative relaxation on the nanoparticle's surface could be considered as one of the most relevant competing relaxation channels in nanoparticles. Obviously, surface passivation of YVO_4 nanoparticles by yttrium fluoride layer leads to a suppression of some surface loss centers, and thus, increases the efficiency of the Eu^{3+} emission.

Another competing relaxation pathways is related to radiative relaxation of excited $(VO_4^{3-})^*$ molecular complexes. It is known that an excited $(VO_4^{3-})^*$ molecular complex itself is efficient intrinsic luminescence center in YVO_4. This intrinsic emission stems from $^3T_1-^1A_1$ radiation [1]. Thus, additionally to the Eu^{3+} emission lines shown with high resolution in Fig. 2, the broad intrinsic luminescence has been also detected in the blue spectral range (Fig. 2). This relatively wide emission band at about 450 nm has been observed in the bulk and nanocrystalline samples, while it is negligibly small or even absent in the emission spectrum of the YVO_4:Eu@YF_3 core-shell sample. The position and shape of the intrinsic emission bands in the bulk and nanocrystals are the same at low temperature. On the other hand, the temperature dependence of the intrinsic emission is different for the bulk and the nanopowders (Fig. 3). In the case of nanocrystals, the intrinsic emission band tends to be shifted toward the low energy side if temperature increases, whereas the position of the corresponding band in the bulk remains the same at any temperature. A similar red shift of the emission band is known for other complex oxide compounds taking the form of ABO_4 with A standing for a monovalent alkaline, divalent alkaline earth, or trivalent lanthanide metal ion, and B for W, Mo, V, or P. In accordance to literature [41,55] the red-shifted emission band in ABO_4 materials is related to perturbed or defected metal-oxide molecular complexes. Hence, the red-shifted broad emission band in the nanocrystalline sample stems from $(VO_4^{3-})^*$ molecular complexes, which are close to the nanoparticle's surface.

From the temperature dependence depicted in Fig. 3, furthermore, it is possible to estimate activation energies for thermal quenching of intrinsic emission in bulk and nanocrystals using Mott and Seitz equation (see details in [56]). So, the values of activation energies 59 meV and 35 meV have been obtained for the bulk and nanopowders, respectively. This difference in values of activation energies is an additional evidence that the emission centers being responsible for blue intrinsic emission of the bulk and of the nanocrystals are different: the regular and the surface related $(VO_4)^{3-}$ complexes in bulk and nanocrystals, respectively.

Returning back to the emission spectra in Fig. 2, we would like to note that the intensity of the broad blue emission in respect of the Eu^{3+} line intensity is the highest for the non-covered nanocrystals, while it is absent for the YVO_4:Eu@YF_3 nanocrystals. We could not observe any intrinsic emission for this sample under any excitation in our measurements (up 40 eV). This means that the YF_3 protection shell around the YVO_4:Eu nanoparticle core not only increases the intensity of the Eu^{3+} emission due to passivation of surface loss centers but also because of switching off the relevant competing relaxation channels – the intrinsic luminescence of $(VO_4^{3-})^*$.

We suggest the following scenario to explain the behavior of intrinsic emission in nanosized YVO_4:Eu and core-shell YVO_4:Eu@YF_3 samples. Excited $(VO_4^{3-})^*$ molecular complex is tend to have a quick energy transfer to neighbouring activator ions. Taking into account that $(VO_4)^{3-}$ molecular complexes are a part of the host lattice, obviously, its concentration in any case is higher than the concentration of Eu^{3+}. Since radiative f-f transition on Eu^{3+} is forbidden, furthermore, this process is a relatively slow (please see the decay kinetics below) and each Eu^{3+} ion cannot accept energy again while being in the excited state. There are some residual excited $(VO_4^{3-})^*$ complexes that relax radiatively in the bulk sample leading to the blue intrinsic emission band (Fig. 2(a)). On the other hand, energy transfer from $(VO_4^{3-})^*$ complexes to Eu^{3+} ions is restricted by the size of the nanocrystallites. Some amount of excited $(VO_4^{3-})^*$ centers are able to transfer energy to the nearest Eu^{3+} ions only, whereas a long-distance energy transfer is restricted in the nanoparticles. The energy transfer occurs via similar $(VO_4^{3-})^*$ complexes, however, surface allocated $(VO_4^{3-})^*$ complexes are perturbed by surface, and therefore, they are distinguished from the corresponding volume complexes. Altogether, surface $(VO_4^{3-})^*$ complexes terminate the energy transfer, i.e., by reaching surface $(VO_4^{3-})^*$ complexes, radiative decay takes place producing the broad blue emission band (Fig. 2(b)). The energy transfer via $(VO_4^{3-})^*$ centers is quick but the nanoparticle size is small, so that the probability of energy transfer to Eu^{3+} or to the nanoparticle's surface is more-or-less similar. Hence, the intensities of the Eu^{3+} and blue emissions are comparable (Fig. 2(b)).

The absence of the intrinsic emission band in YVO:Eu@YF_3 nanoparticles can be explained by the similarity between surface and volume $(VO_4)^{3-}$ centers. Thus, excited $(VO_4^{3-})^*$ centers near the core surface do not terminate the energy transfer any longer, but they can still transfer energy back to neighboured $(VO_4^{3-})^*$ complexes in the

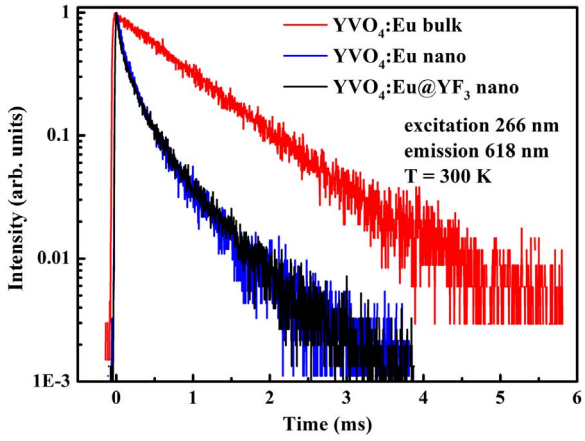

Fig. 4. The decay kinetics of Eu^{3+} emission in three YVO_4:Eu^{3+} samples: bulk, nanocrystals, and core-shell layered nanocrystals. (For interpretation of the references to color in this figure, the reader is referred to the web version of this article.)

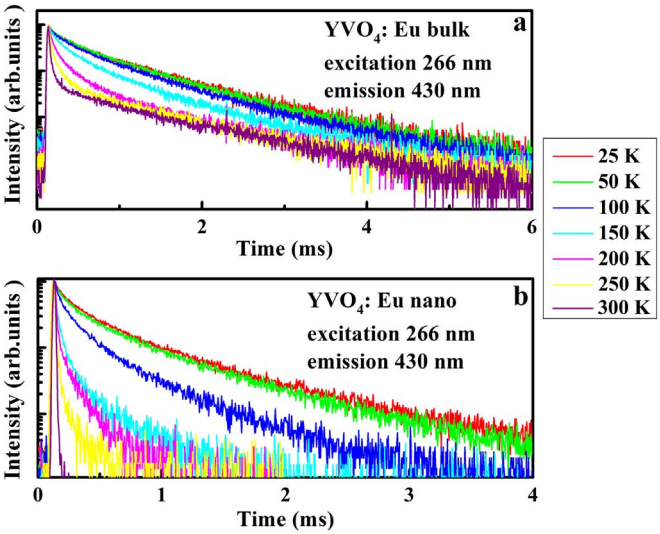

Fig. 5. The temperature dependence of the decay kinetics of intrinsic blue emission in bulk (a) and nanocrystalline (b) YVO_4:Eu^{3+}.

nanoparticle volume until non-excited Eu^{3+} ion is found. Due to the small size of the nanocrystals, the probability of energy transfer to Eu^{3+} ions with such conditions is very high. Our model successfully explains the absence of the blue intrinsic emission and the simultaneous increase of the intensity of Eu^{3+} in the emission spectrum of core-shell layered YVO_4:Eu@YF_3 depicted in Fig. 2(c).

3.2. Time-resolved luminescence

The comparison of the decay kinetics of Eu^{3+} emission under 266 nm excitation at room temperature for bulk, nanocrystalline and core-shell nanocrystalline YVO_4:Eu is given in Fig. 4. It is important to note that the decay kinetics of the Eu^{3+} luminescence does not depend on the temperature in contrast to the decay kinetics of the intrinsic emission (see below). The decay kinetics of the bulk sample (Fig. 4) is exponential with constant decay time of about 1 ms, which is typical for Eu^{3+} luminescence [2]. On the other hand, the decay kinetics of Eu^{3+} luminescence in both uncoated and core-shell layered nanocrystalline samples do not obey the single exponential law. These two decay kinetics (black and blue lines in Fig. 4) are identical and significantly faster than the corresponding decay kinetics of bulk-YVO_4:Eu. This finding can be explained by an energy transfer from the excited state of Eu^{3+} to quench centers as discussed before for many nanophosphors [10,57]. The origin and the specific nature of these surface loss centers are unknown. Due to the similarity of the decay kinetics of Eu^{3+} emission for the uncoated and the core-shell YVO_4:Eu nanoparticles, however, we can suppose that the YF_3 core-shell structure does not remove surface loss centers resulting in this decay-kinetics shortening. This means that the recovery of the Eu^{3+} emission intensity (Fig. 1) in core-shell nanoparticles is achieved at the expense of the suppression of the intrinsic $(VO_4)^{3-}$ emission and not due to the passivation of surface loss centers..

In contrast to the Eu^{3+} decay kinetics (Fig. 4), the decay kinetics of the blue intrinsic emission are temperature dependent for both bulk and nanocrystals (Fig. 5). Fig. 5 demonstrates the normalized decay kinetics of the intrinsic emission for bulk and nanosized YVO_4:Eu under 266 nm laser excitation. These decay kinetics are non-exponential at any temperature. This result contradicts to the data of YVO_4 single crystals where intrinsic luminescence has a single exponential decay in a wide temperature range [58]. A deviation from a single exponential decay means that both bulk and nanosized samples exhibit non-radiative relaxation centers. When increasing the temperature, the probability of non-radiative transitions increases and the decay kinetics of the intrinsic luminescence becomes faster. However, it is clearly visible from Fig. 5 that the temperature quenching is much more pronounced for the nanocrystalline sample where the decay kinetics shortening starts already at temperatures higher than 50 K, whereas the threshold for the temperature quenching of bulk-YVO_4:Eu is higher than 100 K. Accordingly, non-radiative relaxation centers (most likely surface loss centers) play a more significant role for the intrinsic luminescence degradation of the nanocrystalline samples rather than for the bulk sample. Taking into account that the blue intrinsic emission of the nanocrystals stems from surface-allocated $(VO_4)^{3-}$ complexes, the decay kinetics behavior in Fig. 5 is consistently explained..

3.3. Excitation spectra

Excitation spectra in the UV and VUV spectral range of the Eu^{3+} emission of all three samples are depicted in Fig. 6. These spectra are normalized on maximum for better comparison. The excitation spectra of the bulk sample (red line in Fig. 6) reveal a number of excitation peaks in the low energy part, thus, at 4 eV, 5 eV, 6 eV, 9 eV and 12 eV. The first two excitation peaks are as well detected in the excitation spectra of both nanocrystalline samples, whereas the latter three peaks are poorly resolved. In accordance with literature, all these peaks stem from molecular transitions on the $(VO_4^{3-})^*$ complex [2]. The low

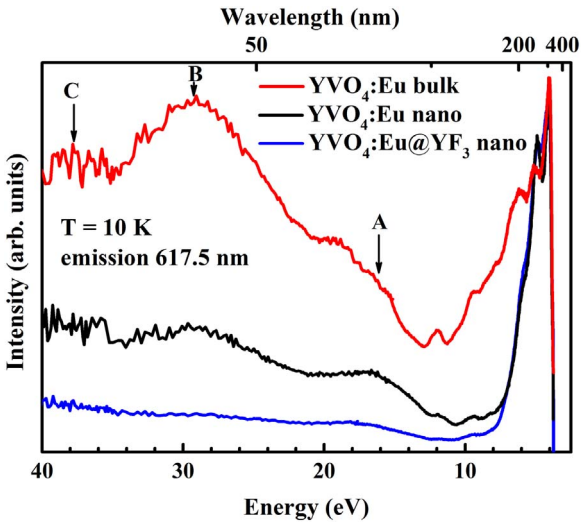

Fig. 6. The excitation spectra of Eu^{3+} emission in three YVO_4:Eu^{3+} samples: bulk, nanocrystals, and core-shell layered nanocrystals. (For interpretation of the references to color in this figure, the reader is referred to the web version of this article.)

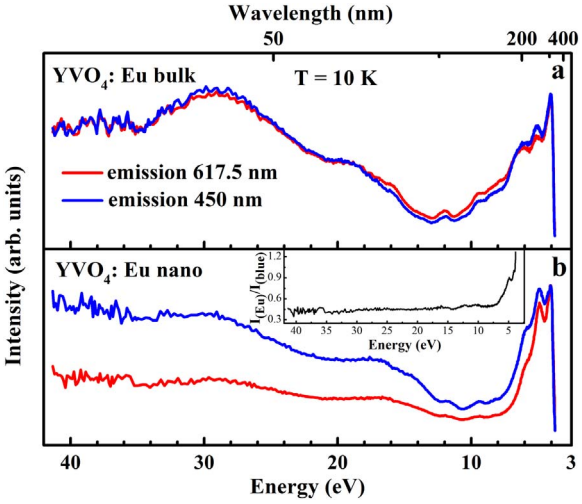

Fig. 7. The comparison of the excitation spectra of Eu^{3+} and intrinsic emissions in bulk (a) and nanocrystalline (b) YVO_4:Eu^{3+}. The inset in (b) shows the ratio of two spectra.

intensity of the high-energy transitions (excitation peaks at 6 eV, 9 eV and 12 eV) could be explained by the perturbation of high-energy molecular states by nanoparticle surface.

At energies higher than 12 eV, the excitation spectra of the bulk and of uncovered nanocrystalline YVO_4:Eu are similar. Each spectrum contains three broad excitation bands marked as A, B and C (Fig. 6). The most intensive peak B can be attributed to the transition from 4p orbitals of Y^{3+} to the conduction band [2]. Similar excitation peaks at about 30 eV are known for other yttrium containing compounds [59–61]. The high-energy peak C, in fact, is a tail of the excitation peak at 45–50 eV, which demonstrates the transition from vanadium 4p states to the conduction band [2]. The peak A can be assigned to a plasmon excitation [2]. All three high-energy peaks (A, B and C) are significantly more intensive for the bulk sample. Indeed, the intensity of the excitation peak B of nanosized YVO_4:Eu is about 30% less intense and about 10% less intense for core-shell YVO_4:Eu@YF_3 in comparison to bulk-YVO_4:Eu. The reduction of the excitation spectrum of nanosized YVO_4:Eu could be explained by surface trapping of hot electrons, which were excited from yttrium and vanadium core orbitals to the conduction band. The surface passivation of core shell YVO_4:Eu@YF_3 samples does not help to increase the intensity of the excitation peak in the 12–45 eV range. Since the band-gap energy of the YF_3 shell is about 11 eV [59], it is supposed that the YF_3 shell around YVO_4:Eu nanoparticles serves as a "shield" that partially absorbs the excitation energy.

Fig. 7 confirms the tendency of the surface relaxation under high-energy excitation. This figure demonstrates the comparison of the excitation spectra of impurity (Eu^{3+}) and intrinsic (blue) emissions in bulk (a) and nanocrystalline (b) YVO_4:Eu^{3+}. It is clearly seen that the excitation spectra of the two emissions of the bulk sample are identical (Fig. 7(a)), whereas the efficiency of Eu^{3+} emission is significantly lower than the efficiency of the intrinsic emission. The most prominent difference between the efficiency of Eu^{3+} and the intrinsic emissions is observed in the 10–40 eV spectral range. The inset of Fig. 7(b) shows the intensity ratio of the Eu^{3+} emission and the intrinsic emission. The ratio $I_{(Eu)}/I_{(intrinsic)}$ drops below 0.5 in the 10–40 eV spectral range. This is an additional argument demonstrating that electrons and holes in the nanoparticles under high-energy excitation tend to be trapped by surface defects with subsequent relaxation via radiative recombination within $(VO_4^{3-})^*$ complexes. Such process represents a competing relaxation channel to the radiative relaxation on Eu^{3+} ions and, therefore, leads to a reduction of the Eu^{3+} emission under high-energy excitation..

4. Conclusions

The comparative analysis of bulk-YVO_4:Eu, uncoated nanocrystalline YVO_4:Eu and core-shell YVO_4@YF_3 nanocrystalls has been performed by means of time-resolved luminescence and VUV luminescence spectroscopy techniques. The main focus this study were paid to the influence of the nanoparticle surface on the luminescence processes in YVO_4:Eu and the role of the YF_3 shell regarding the Eu^{3+} emission. The results can be summarized as follows:

1) Additionally to Eu^{3+} emission a blue intrinsic emission band has been observed for bulk and nanocrystalline YVO_4:Eu. Despite of the similarity of the blue emission the responsible emission centers are different in bulk material and nanocrystals. The $(VO_4^{3-})^*$ molecular complex on the nanoparticle's surface is the origin of this blue intrinsic emission in nanocrystals, whereas regular lattice $(VO_4^{3-})^*$ molecular complexes are well-known emission center in bulk-YVO_4. The blue intrinsic emission stemmed from surface related $(VO_4)^{3-}$ molecular complex in nanocrystals is a strong relaxation channel, which competes with the Eu^{3+} emission. It is suggested that efficient blue emission is one of the reasons of a strong degradation of the Eu^{3+} luminescence in YVO_4:Eu nanocrystals.
2) The intrinsic blue emission is absent in core-shell YVO_4@YF_3 nanocrystals. It is suggested that the YF_3 shell around the YVO_4:Eu nanoparticles transforms the surface related $(VO_4^{3-})^*$ into regular one switching off a strong competing relaxation channel. This is a main reason of a strong recovery of intensity of Eu^{3+} luminescence of the core-shell YVO_4:Eu@YF_3 nanocrystalls.
3) The efficiency of the energy transfer from host lattice to the Eu^{3+} ions depends on the excitation energy. It is suggested that surface loss processes, namely electron-hole non-radiative relaxation as well as a radiative relaxation within surface related $(VO_4^{3-})^*$ molecular complexes, are the reason of the degradation of energy-transfer efficiency from host lattice to Eu^{3+} under high energy excitations. This fact definitely restricts the use of nanocrystalline YVO_4:Eu as a phosphor for the transformation of high energy excitations into visible light.

Acknowledgements

V.P. acknowledges the financial supports from Oulu University Strategic Funding and Research Council for Natural Sciences of the Academy of Finland. The research leading to these results has received funding from the European Community's Seventh Framework Programme (FP7/2007–2013) CALIPSO under Grant agreement no. 312284. Authors also thankful to Dr. A. Sarakovskis (Institute of Solid State Physics, University of Latvia) in his assistance for time-resolved luminescence spectroscopy experiments.

References

[1] A.K. Levine, F.C. Palilla, A new, highly efficient red-emitting chatodoluminescent phosphor (YVO_4: Eu) for color television, Appl. Phys. Lett. 5 (1964) 118–120.
[2] W.M. Yen, S. Shionoya, H. Yamamoto, Phosphor Handbook, 2nd edition, CRC Press, Boca-Raton, 1999.
[3] A. Bril, W.L. Wanmaker, J. Broos, Photoluminescent properties of some europium-activated gadolinium and yttrium compounds, J. Chem. Phys. 43 (1965) (311-311).
[4] L.R. Singh, R.S. Ningthoujam, Critical view on energy transfer, site symmetry, improvement in luminescence of Eu^{3+}, Dy^{3+} doped YVO_4 by core-shell formation, J. Appl. Phys. 107 (2010) 104304–104306.
[5] C. Hsu, R.C. Powell, Energy transfer in europium doped yttrium vanadate crystals, J. Lumin. 10 (1975) 273–293.
[6] E.D. Reed Jr., H. Warren Warren Moos, Moos, Nonthermalization and large variation in multiphonon relaxation rate among rare-earth-ion Stark levels, Phys. Rev. B 8 (1973) 988–992.
[7] C.P. Frank, L. Albert, R. Maija, Synthesis and luminescent properties of $LaVO_4$:Re nanocrystals, J. Electrochem. Soc. 112 (1965) 776–781.
[8] U. Rambabu, D.P. Amalnerkar, B.B. Kale, S. Buddhudu, Fluorescence spectra of Eu^{3+}-doped $LnVO_4$ (Ln=La and Y) powder phosphors, Mater. Res. Bull. 35 (2000) 929–936.

[9] C. Brecher, H. Samelson, A. Lempicki, R. Riley, T. Peters, Polarized spectra and crystal-field parameters of Eu^{3+} in YVO_4, Phys. Rev. 155 (1967) 178–187.
[10] K. Riwotzki, M. Haase, Colloidal YVO_4:Eu and $YP_{0.95}V_{0.05}O_4$:Eu nanoparticles: luminescence and energy transfer processes, J. Phys. Chem. B 105 (2001) 12709–12713.
[11] A. Huignard, T. Gacoin, J.-P. Boilot, Synthesis and luminescence properties of colloidal YVO_4:Eu phosphors, Chem. Mater. 12 (2000) 1090–1094.
[12] K. Riwotzki, M. Haase, Wet-Chemical Synthesis of Doped Colloidal Nanoparticles: YVO_4:Ln (Ln=Eu, Sm, Dy), J. Phys. Chem. B 102 (1998) 10129–10135.
[13] W. Xu, Y. Wang, X. Bai, B. Dong, Q. Liu, J. Chen, H. Song, Controllable synthesis and size-dependent luminescent properties of YVO_4:Eu^{3+} nanospheres and microspheres, J. Phys. Chem. C 114 (2010) 14018–14024.
[14] M. Wu, S. Choi, H.-K. Jung, Preparation of transparent red-emitting layer using hydrothermally synthesized YVO_4:Eu^{3+} nanophosphors, Mater. Res. Bull. 78 (2016) 20–25.
[15] H. Wang, O. Odawara, H. Wada, Facile and chemically pure preparation of YVO_4:Eu^{3+} colloid with novel nanostructure via laser ablation in water, Sci. Rep. 6 (2016) 20507.
[16] M.S. Rabasovic, J. Krizan, P. Gregorcic, M.D. Rabasovic, N. Romcevic, D. Sevic, Time-resolved luminescence spectra of Eu^{3+} doped YVO_4, Sr_2CeO_4 and $Gd_2Zr_2O_7$ nanopowders, Opt. Quant. Electron 48 (2016) 163.
[17] Y. Liu, H. Xiong, N. Zhang, Z. Leng, R. Li, S. Gan, Microwave synthesis and luminescent properties of YVO_4:Ln^{3+}(Ln=Eu, Dy and Sm) phosphors with different morphologies, J. Alloy. Compd. 653 (2015) 126–134.
[18] E.V. Tomina, B.V. Sladkopevtsev, V.O. Mittova, M.V. Knurova, A.N. Latyshev, I. Ya, Microwave synthesis and luminescence properties of YVO_4:Eu^{3+}, Inorg. Mater 52 (2016) 495.
[19] B.F. dos Santos Jr., R.M. Araujo, M.E.G. Valerio, M.V. dos, S. Rezende, Optical spectroscopy study of YVO_4:Eu^{3+} nanopowders prepared by the proteic sol–gel route, Solid State Sci. 42 (2015) 45–51.
[20] E.V. Golyeva, D.V. Tolstikova, I.E. Kolesnikov, M.D. Mikhailov, Effect Of Synthesis Conditions And Surrounding Medium On Luminescence Properties Of YVO_4:Eu^{3+} Nanopowders, J. Rare Earth. 33 (2015) 129–134.
[21] I.E. Kolesnikov, D.V. Tolstikova, A.V. Kurochkin, S.A. Pulkin, A.A. Manshina, M.D. Mikhailov, Concentration effect on photoluminescence of Eu^{3+}-doped nanocrystalline YVO_4, J. Lumin. 158 (2015) 469–474.
[22] L. Lina, X. Hongyu, A. Xiuyun, Z. Yongsheng, Q. Ruifei, L. Lishuang, Z. Dongmei, S. Ruirui, C. Linfeng, Synthesis and photoluminescence properties of core-shell structured YVO_4:Eu^{3+}@SiO_2 nanocomposites, Chem. Phys. Lett. 619 (2015) 169–173.
[23] N. Martinez, T. Teichmann, P. Molina, M. Sommer, M. Santiago, J. Henniger, E. Caselli, Scintillation properties of the YVO_4:Eu^{3+} compound in powder form: its application to dosimetry in radiation fields produced by pulsed mega-voltage photon beams, Z. Med. Phys. 25 (2015) 368–374.
[24] L. Liu, S. Yue, Y. Zhang, R. Qin, L. Liu, D. Zhang, R. Sun, L. Chen, One-pot reverse microemulsion synthesis of core–shell structured YVO_4:Eu^{3+}@SiO_2 nanocomposites, Opt. Mater. 39 (2015) 207–2010.
[25] M. Nakamura, K. Chida, M. Zuguchi, Red emission phosphor for real-time skin dosimeter for fluoroscopy and interventional radiology, Med. Phys. 41 (2014) 101913.
[26] N. Shanta Singh, H. Kulkarni, L. Pradhan, D. Bahadur, A multifunctional biphasic suspension of mesoporous silica encapsulated with YVO_4:Eu^{3+} and Fe_3O_4 nanoparticles: synergistic effect towards cancer therapy and imaging, Nanotechnology 24 (2013) 065101.
[27] H. Goesmann, C. Feldmann, Nanoparticulate functional materials, Angew. Chem. Int. Ed. 49 (2010) 1362–1395.
[28] H. Althues, J. Henle, S. Kaskel, Functional inorganic nanofillers for transparent polymers, Chem. Soc. Rev. 36 (2007) 1454–1465.
[29] M. Bruchez, M. Moronne, P. Gin, S. Weiss, A.P. Alivisatos, Semiconductor nanocrystals as fluorescent biological labels, Science 281 (1998) 2013–2016.
[30] T. Pellegrino, S. Kudera, T. Liedl, A. Munoz Javier, L. Manna, W. Parak, On the devolpment of colloidal naarticles towards multifunctional structures and their possible use for biological application, Small 1 (2005) 48–63.
[31] M. Yu, J. Lin, Z. Wang, J. Fu, S. Wang, H.J. Zhang, Y.C. Han, Fabrication, patterning, and optical properties of nanocrystalline YVO_4:A (A=Eu^{3+}, Dy^{3+}, Sm^{3+}, Er^{3+}) phosphor films via sol-gel soft lithography, Chem. Mater. 14 (2002) 2224–2231.
[32] H. Yuan, Y. Qiao, H. Yang, Preparation and luminescent properties of doped with Eu^{3+} ions YVO_4 nanophosphors, J. Mater. Sci. -Mater. El 25 (2014) 4001–4003.
[33] S. Ekambaram, K.C. Patil, Rapid synthesis and properties of $FeVO_4$, $AlVO_4$, YVO_4 and Eu^{3+}-doped YVO_4, J. Alloy. Compd. 217 (1995) 104–107.
[34] L.D. Sun, Y.X. Zhang, J. Zhang, C.H. Yan, C.S. Liao, Y.Q. Lu, Fabrication of size controllable YVO_4 nanoparticles via microemulsion-mediated synthetic process, Solid State Commun. 124 (2002) 35–38.
[35] Y.H. Li, G.Y. Hong, Synthesis and luminescence properties of nanocrystalline YVO_4:Eu^{3+}, J. Solid State Chem. 175 (2005) 645–649.
[36] G. Jia, Y. Song, Mei Yang, Y. Huang, L. Zhang, H. You, Uniform YVO_4:Ln^{3+}(Ln=Eu, Dy, and Sm) nanocrystals: solvothermal synthesisand luminescence properties, Opt. Mater. 31 (2009) 1032–1037.
[37] A. Huignard, V. Buissette, G. Laurent, T. Gacoin, J.-P. Boilot, Synthesis and characterizations of YVO_4:Eu colloids, Chem. Mater. 14 (2002) 2264–2269.
[38] N. Duée, C. Ambard, F. Pereira, D. Portehault, B. Viana, K. Vallé, D. Autissier, C. Sanchez, New Synthesis Strategies for Luminescent YVO_4:Eu and $EuVO_4$ Nanoparticles with H_2O_2 Selective Sensing Properties, Chem. Mater. 27 (2015) 5198–5205.
[39] C. Feldmann, T. Justel, C.R. Ronda, P.J. Schmidt, Inorganic luminescent materials: 100 years of research and application, Adv. Funct. Mater. 13 (2003) 511–516.
[40] A. Zharkouskay, H. Lunsdorf, C. Feldmann, Ionic liquid-based synthesis of luminescent YVO_4:Eu and YVO_4:Eu@YF_3 nanocrystals, J. Mater. Sci. 44 (2009) 3936–3942.
[41] A. Kuzmanoski, V. Pankratov, C. Feldmann, Microwave-assisted ionic-liquid-based synthesis of highly crystalline $CaMoO_4$:RE^{3+}(RE=Tb, Sm, Eu) and $Y_2Mo_4O_{15}$:Eu^{3+} nanoparticles, Solid State Sci. 41 (2015) 56–62.
[42] A. Tuomela, V. Pankratov, A. Sarakovskis, G. Doke, L. Grinberga, S. Vielhauer, M. Huttula, Oxygen influence on luminescence properties of rare-earth doped $NaLaF_4$, J. Lumin. 179 (2016) 16–20.
[43] P.V. Savchyn, V.V. Vistovskyya, A.S. Pushak, A.S. Voloshinovskii, A.V. Gektin, V. Pankratov, A.I. Popov, Synchrotron radiation studies on luminescence of Eu^{2+}-doped $LaCl_3$ microcrystals embedded in a NaCl matrix, Nucl. Instrum. Methods B 274 (2012) 78–82.
[44] H.H. Rüter, H. v Seggern, R. Reininger, V. Saile, Creation of photostimulable centers in BaFBr:Eu^{2+} single crystals by vacuum ultraviolet radiation, Phys. Rev. Lett. 65 (1990) 2438–2441.
[45] V. Pankratov, A.I. Popov, L. Shirmane, A. Kotlov, G.A. Bizarri, A. Burger, P. Bhattacharya, E. Tupitsyn, E. Rowe, V.M. Buliga, R.T. Williams, Luminescence and ultraviolet excitation spectroscopy of SrI_2 and SrI_2:Eu^{2+}, Radiat. Meas. 56 (2013) 13–17.
[46] V. Pankratov, L. Grigorjeva, S. Chernov, T. Chudoba, W. Lojkowski, Luminescence properties and energy transfer processes in nanosized cerium doped YAG, IEEE Trans. Nucl. Sci. 55 (2008) 1509–1513.
[47] V. Pankratov, A.I. Popov, L. Shirmane, A. Kotlov, C. Feldmann, $LaPO_4$:Ce, Tb and YVO_4:Eu nanophosphors: luminescence studies in the vacuum ultraviolet spectral range, J. Appl. Phys. 110 (2011) 053522.
[48] L. Shirmane, V. Pankratov, Emerging blue-UV luminescence in cerium doped YAG nanocrystals, Phys. Status Solidi RLL 10 (2016) 475–479.
[49] V. Pankratov, V. Osinniy, A. Kotlov, A. Nylandsted Larsen, B. Bech Nielsen, Si nanocrystals embedded in SiO_2: optical studies in the vacuum ultraviolet range, Phys. Rev. B 83 (2011) 045308.
[50] V. Pankratov, J. Hoszowska, J.-Cl Dousse, M. Huttula, A. Kis, D. Krasnozhon, M. Zhang, W. Cao, Vacuum ultraviolet excitation luminescence spectroscopy of few-layered MoS_2, J. Phys. Condens Matter 28 (2015) 015301.
[51] G. Zimmerer, Superlumi: a unique setup for luminescence spectroscopy with synchrotron radiation, Radiat. Meas. 42 (2007) 859–864.
[52] S. Urpelainen, M. Huttula, T. Balasubramanian, R. Sankari, P. Kovala, E. Kukk, E. Nõmmiste, S. Aksela, R. Nyholm, H. Aksela, FINEST: a high performance branchline for VUV photon energy range gas phase studies at MAX-lab, in: AIP Conference Proceedings, vol. 1234, 2010. (411-414).
[53] T. Balasubramanian, B.N. Jensen, S. Urpelainen, B. Sommarin, U. Johansson, M. Huttula, R. Sankari, E. Nõmmiste, S. Aksela, H. Aksela, R. Nyholm, The normal incidence monochromator beamline I3 on MAX III, in: AIP Conference Proceedings, vol. 1234, 2010, pp. 661–664.
[54] M.R. Dolgos, A.M. Paraskos, M.W. Stoltzfus, S.C. Yarnell, P.M. Woodward, The electronic structures of vanadate salts: cation substitution as a tool for band gap manipulation, J. Solid State Chem. 182 (2009) 1964–1971.
[55] D. Millers, S. Chernov, L. Grigorjeva, V. Pankratov, The energy transfer to the luminescence centers in $PbWO_4$, Radiat. Meas. 29 (1998) 263–266.
[56] V. Pankratov, L. Grigorjeva, D. Millers, H.M. Yochum, Intrinsic luminescence and energy transfer processes in pure and doped YVO_4 crystals, Phys. Status Solidi 4 (2007) 801–804.
[57] V. Pankratov, D. Millers, L. Grigorjeva, W. Lojkowski, A. Kareiva, Time-resolved luminescence of nanocrystalline inorganic complex oxides, J. Phys. Conf. Ser 93 (2007) 012037.
[58] W. Ryba-Romanowski, S. Golab, P. Solarz, G. Dominiak-Dzik, T. Lukasiewicz, Anti-Stokes emission in undoped YVO_4, Appl. Phys. Lett. 80 (2002) 1183–1185.
[59] V. Pankratov, M. Kirm, H. von Seggern, Exciton emission and defect formation in yttrium trifluoride, Phys. Status Solidi C 2 (2005) 371–374.
[60] M. Kirm, A. Lushchik, Ch. Lushchik, G. Zimmerer, Investigation of luminescence properties of pure and Ce^{3+} Doped $Y_3Al_5O_{12}$ crystals using VUV radiation, Elec. Soc. S., 99-40, 2000, pp. 113–122.
[61] T. Tomiki, F. Fukudome, M. Kaminao, M. Fujisawa, Y. Tanahara, T. Futemma, Optical properties of YAG and YAP single crystals in VUV, J. Lumin. 40–41 (1988) 379–380.

Phys. Status Solidi RRL **10**, No. 6, 475–479 (2016) / **DOI** 10.1002/pssr.201600041

pss +++rapid research letters+++
www.pss-rapid.com

Emerging blue-UV luminescence in cerium doped YAG nanocrystals

Liana Shirmane[**,1] **and Vladimir Pankratov**[*,2]

[1] Institute of Solid State Physics, University of Latvia, Kengaraga iela 8, 1063 Riga, Latvia
[2] Research Center of Molecular Materials, University of Oulu, P.O. Box 3000, 90014 Oulu, Finland

Received 14 February 2016, revised 12 April 2016, accepted 18 April 2016
Published online 22 April 2016

Keywords Ce^{3+}, YAG, phosphors, scintillators, luminescence, VUV spectroscopy, synchrotron radiation

[*] Corresponding author: e-mail vladimirs.pankratovs@oulu.fi, Phone: +358 50 4315681
[**] e-mail liana.shirmane@gmail.com

Time-resolved luminescence properties of Ce^{3+} doped $Y_3Al_5O_{12}$ (YAG) nanocrystals have been studied by means of vacuum-ultraviolet excitation spectroscopy. It was discovered that additionally to the regular Ce^{3+} yellow-green emission which is well-known luminescence in YAG, new emission covering a broad spectral range from 2.7 eV to 3.5 eV was revealed in the luminescence spectra for all YAG:Ce nanocrystals studied. This blue-UV emission has fast decay time about 7 ns as well as intensive well-resolved excitation band peaking at 5.9 eV and, in contrast to green Ce^{3+} emission, practically is not excited at higher energies. The origin of the blue-UV emission is tentatively suggested and discussed.

1 Introduction Bulk cerium doped $Y_3Al_5O_{12}$ (YAG:Ce) is an important and well-known luminescent material that had been studied for more than 40 years. This compound became as one of the most popular materials among others because of its high radiation and chemical stability as well as efficient yellow-green luminescence ([1, 2] and references therein). Luminescent nanocrystals or nanophosphors (including YAG:Ce) recently received increased attention because of their potential application in medicine and biophysics (labeling, signaling, and biomedical purpose) [3]. Generally, nanophosphors of various inorganic compounds in form of nanopowders and nanoceramics have been successfully synthesized during the last decade all over the world thanks to rapidly developed nanotechnologies. It was reported that YAG:Ce nanopowders have been successfully synthesized by means of many techniques, which include co-precipitation method [4], hydrothermal process [5], Pechini method [6], sol–gel method [7]. Resent researches of YAG:Ce are mostly focused on the synthesis, characterization and applications of YAG:Ce in form of nanopowders [8, 9], nanoceramics [10–13] and single crystalline films [14, 15].

The main goal of the current investigation is a study of the luminescence properties of nanosized YAG:Ce under high energy excitations including vacuum ultraviolet (VUV) range, which is important for biolabelling, radiation therapy applications and scintillators. In our study we applied synchrotron radiation, which has significant advantages over the radiation of ordinary sources. The main advantages of synchrotron radiation are the extended wavelength range attained, that gives broad and continuous spectrum. In recent works it was shown how important is to use synchrotron radiation in investigation of optical and luminescence properties of wide band gap insulators [9, 16–20] as well as of nanocrystalline and two-dimensional semiconductors [21, 22].

2 Results and discussion The luminescence measurements were carried out using pulsed synchrotron radiation at the Superlumi station at Photon Science (DESY, Hamburg) [23]. Luminescence spectra in the UV and visible range were recorded with a spectrograph SpectraPro-308i (Acton Research Corporation) equipped with a photomultiplier (Hamamatsu R6358P). The spectral resolution of the analysing monochromator was typically 11 nm. Emission spectra were corrected for the spectral response of the detection systems. The excitation spectra were recorded with spectral resolution of 0.3 nm. The excitation spectra were normalized to equal quantum intensities of synchrotron radiation falling onto sample by means of sodium salicylate as reference. The exciting pulse duration is 125 ps, while the instrumental time resolution of the regis-

tration system was 1 ns. Emission decay kinetics have been measured in 196 ns time window. All experiments were carried out at room temperature.

YAG:Ce nanopowders have been synthesized by means of a modified sol–gel method similar to that used by Pechini, which described in details elsewhere [24]. The nanopowders were characterized by means of Scherrer method, Williamson–Hall method, X-ray powder diffraction and BET methods [10]. The average particle size was estimated to be about 20 nm. Cerium ions concentration in YAG:Ce nanopowders varied from 0.5% to 5.0%.

The luminescence spectra of YAG:Ce nanopowders under high energy excitation (exceeding band gap energy of YAG) are shown in Fig. 1(a–e). In these figures one can see that all spectra demonstrate only yellow-green emission of regular Ce^{3+} in YAG. There are no significant differences in the spectra shapes depending on Ce^{3+} concentration. The emission spectrum for the single crystal (Fig. 1(f)) also does not reveal any principle differences compared to the emission spectra of the nanopowders. On the other hand, the emission spectra of YAG:Ce nanopowders are drastically changed if excitation energy is below the band gap energy of YAG. In this case, additionally to the yellow-green emission of the regular Ce^{3+} (peaking at 520 nm) an intensive emission in the blue-UV spectral range was observed in all nanopowders studied under 210 nm (5.9 eV) excitation (Fig. 1(g–l)). The intensity of the blue-UV depends on Ce^{3+} concentration in the YAG nanopowders. One can see that this emission can reach up to 75% of the intensity of the regular Ce^{3+} emission in 0.5% doped nanopowder and it suppresses strongly if Ce^{3+} concentration in nanopowders increases from 0.5% to 5%. It is important to note that in contrast to nanopowders, only the regular Ce^{3+} emission band with maximum at 2.4 eV (520 nm) was detected for single crystal under any excitations.

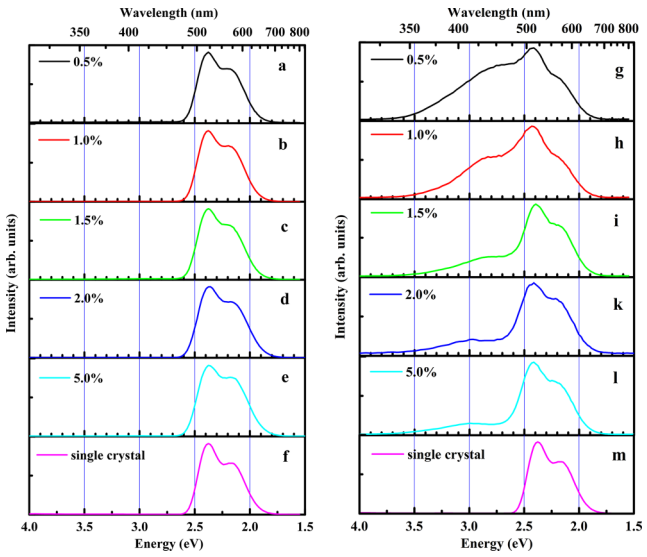

Figure 1 Emission spectra of YAG:Ce nanopowders having different Ce^{3+} content under 115 nm (10.78 eV) (a–e) and 210 nm (5.9 eV) (g–l) excitations. The luminescence spectra of the YAG:Ce single crystal under corresponding excitations are given for comparison (f, m). All spectra are scaled at 520 nm (2.4 eV).

The excitation spectra for the regular yellow-green Ce^{3+} emission in one of YAG:Ce nanopowders (0.5% Ce^{3+} concentration) as well as in the single crystal are shown in Fig. 2(a), while Fig. 2(b) depicts the excitation spectrum of the blue-UV (at 400 nm) emission observed in one of the nanopowdered samples (also 0.5% Ce^{3+} concentration). Note, the excitation spectra in Fig. 2 are typical for all nanopowders studied and their shapes are poorly cerium concentration dependent. The excitation spectrum of the regular Ce^{3+} emission in the single crystal reveals several excitation bands in the transparency region of YAG (Fig. 2(a)): ~340 nm (3.7 eV), 270 nm (4.59 eV), 220 nm (5.6 eV), and 205 nm (6.05 eV) (see arrows in Fig. 2(a)). These excitation bands in YAG:Ce^{3+} have been reported in many studies before and the peak maxima, which depend to some extent upon temperature and the concentration of Ce^{3+} are analysed in detail in [9, 25–27]. These excitation peaks stem from the splitting of $5d^1$ excited state of Ce^{3+} in the crystalline field of D_2 symmetry, when Ce^{3+} ion is incorporated into the YAG lattice substituting Y^{3+} ion. The corresponding excitation bands of the regular Ce^{3+} emission in nanopowders are poorly resolved due to their increased broadening. Therefore, the excitation spectrum represents a broad shapeless band (blue dashed line in

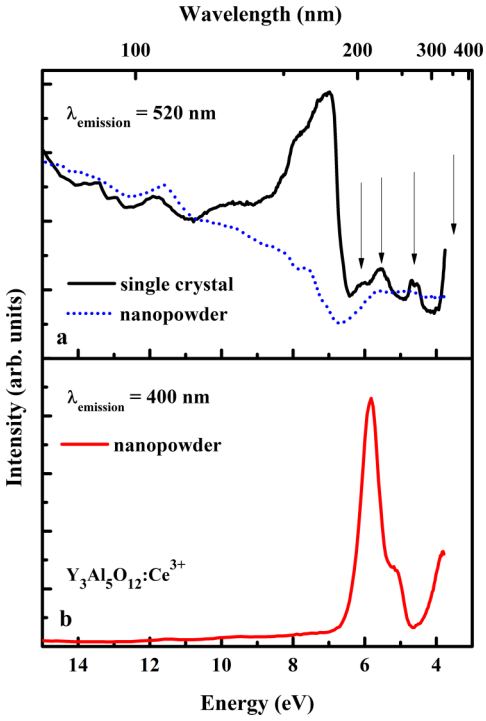

Figure 2 Excitation spectra of the regular Ce^{3+} emission in YAG:Ce single crystal and one of nanopowders (0.5%) (a). Excitation spectrum of the blue-UV emission band in one of the YAG:Ce nanocrystalline samples (0.5%) (b). The arrows in (a) indicate the spectral positions of regular Ce^{3+} excitation peaks known in literature for bulk YAG:Ce (see details in the text).

Fig. 2(a)) covering a spectral range from 200 nm to 350 nm. Additionally to the excitation bands due to 4f–5d transitions the strong excitation is observed in the excitonic spectral range in YAG:Ce single crystal just below the band gap energy of YAG (8 eV). It is clearly seen (Fig. 2(a)) that excitonic excitations are strongly suppressed in the nanocrystalline sample. This fact was already observed and discussed in detail elsewhere [9]. The excitation curves at energies higher than 8 eV are identical for the single crystal and nanopowders. The excitation spectrum of Ce^{3+} emission in YAG in the 8–40 eV spectral range has been studied in detail in [28] where the rise of Ce^{3+} intensity at energies exceeding 8 eV was explained by the direct impact excitation of Ce^{3+} centers by hot photoelectrons as well as by the multiplications of electronic excitation processes.

The excitation spectrum of blue-UV emission (400 nm) depicted in Fig. 2(b) drastically differs from the excitation spectra of the regular Ce^{3+} emission shown in Fig. 2(a). The excitation spectrum of the blue-UV emission contains a strong main peak at 210 nm (5.9 eV) with the well-resolved shoulder at 240 nm (5.17 eV) and the low energy peak at about 330 nm. The result shown Fig. 2(b) indicates that the excitation spectrum of the blue-UV emission is not comparable with the excitation bands of the regular Ce^{3+} emission observed for both single and nanocrystalline samples in the 4–8 eV spectral range (Fig. 2(a)). Therefore, the excitation spectrum of the blue-UV emission cannot be simply explained in term of crystal field splitting of $5d^1$ state of the regular Ce^{3+} ion.

Another remarkable feature of the excitation spectra of the blue-UV emission (Fig. 2(b)) is that this emission cannot be effectively excited at energies higher than the band gap energy in YAG (8 eV). This experimental result shows that there is extremely weak energy transfer efficiency from YAG lattice to the emission center responsible for the blue-UV emission band in YAG:Ce nanocrystals.

Emission decay kinetics of both regular yellow-green and the blue-UV emissions in YAG:Ce nanocrystals are shown in Fig. 3. The decay kinetic of the regular Ce^{3+} emission observed in the single crystal is shown also in Fig. 3(a) for comparison. It is known that the Ce^{3+} emission in YAG single crystal has a characteristic decay time constant about 80 ns [8]. On the other hand, the decay time constant in nanocrystals usually is faster than in bulk due to non-radiative relaxation induced by surface loss centers which always occur on nanoparticles' surface [8, 29, 30]. Obviously, total decay time of the regular Ce^{3+} emission in the single crystal as well as in the most of nanocrystals (Fig. 3(a)) is much slower than the time window of the registration system. Nevertheless, one can see that there is a strong decay time dependence on Ce^{3+} concentration in YAG:Ce nanocrystals studied: emission decay is faster in those YAG:Ce nanocrystals having a higher Ce^{3+} concentration. This dependence in Fig. 3(a) indicates that increasing Ce^{3+} concentration ions leads to increased number of Ce^{3+} ions on surface sites of nanoparticles where the influence of surface loss centers is strong.

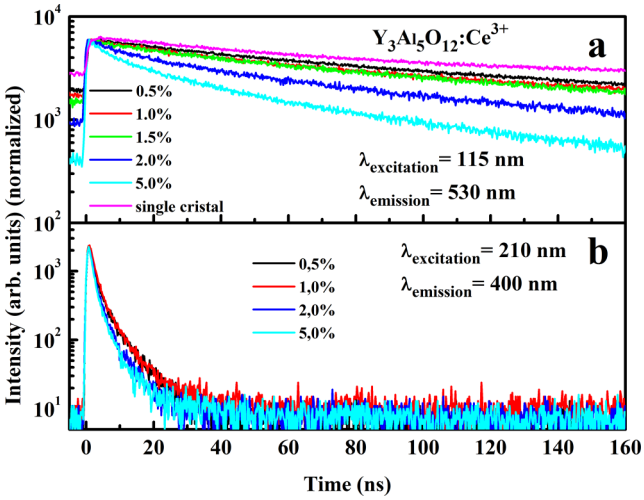

Figure 3 Decay kinetics of the regular yellow-green (a) and the blue-UV (b) emissions for YAG:Ce nanocrystals having different Ce^{3+} concentration. The decay kinetic of the regular yellow-green emission band for the single crystal is given for comparison in (a).

The decay kinetics of the blue-UV emission (Fig. 3(b)) have a completely different behaviour. First, the blue-UV emission decays much faster than the yellow-green one: the decay time constant of the blue-UV emission can be roughly estimated as about 6–8 ns. Secondly, there is not significant dependency of the decay curves displayed in Fig. 3(b) on the Ce^{3+} concentration in the nanocrystals examined.

Distinguished emission and excitation spectra as well as emission decay kinetics observed in YAG:Ce nanocrystals for the yellow-green and the blue-UV emission bands indicate that these emissions belong to the different emission centers. The origin of the yellow-green emission is evident, the regular Ce^{3+} ion substituting Y^{3+} site (Ce_Y^{3+}). Luminescence properties of this center in the nanocrystalline samples can be described and explained adhering to the analogy with the bulk YAG:Ce. On the other hand, the origin of the blue-UV emission center is debatable.

The blue-UV emission obtained in our study should be distinguished from the intrinsic defect-related luminescence known in YAG. The emission band of *antisite* defects and F^+ centers are peaking at 302 nm (4.1 eV) and 390 nm (3.15 eV) respectively [9, 13, 14], while the blue-UV emission in Fig. 1 covers spectral range from 360 nm (3.4 eV) to 460 nm (2.7 eV). Similar emission bands at 3.1 eV and 3.3 eV were observed in YAG:Ce nanocrystals in [8] and [9], respectively. In contrast to the emission shown in Fig. 1 the emissions at 3.1 eV [8] and 3.3 eV [9] were reported for the sample with unknown Ce^{3+} concentration and quality and they were relatively narrow and much weaker than the blue-UV bands shown in Fig. 1. Therefore, we can summarize that to our knowledge the blue-UV luminescence observed in the current study for the YAG:Ce nanocrystals covering a broad spectral range

and having high intensity is not reported in literature before. Taking into account that the XRD analysis did not reveal any difference in structure of the nanocrystals and bulk YAG [10, 11] we suggest that the blue-UV emission occurs due to reduced size of the nanoparticles. The nanoparticle's size is about 20 nm and definitely such nanoparticles cannot induce quantum confinement effects in the nanocrystals studied. However, the contribution of surface drastically increases in nanoparticles having such particle size. Therefore, the nanoparticles can have a significant numbers of specific centers related to the nanoparticle's surface (or located close to the surface), which are not typical for the corresponding bulk material. Furthermore, since the intensity of blue-UV emission depends strongly on the Ce^{3+} concentration (Fig. 1(g–l)) we suggest that the center responsible for the blue-UV emission is Ce^{3+} ion in some specific site of YAG lattice. This specific site for Ce^{3+} ion should be unusual for bulk YAG:Ce because we did not detect the blue-UV emission in the crystal under any excitations (Fig. 1(f, m)). It is suggested that without any charge compensation Ce^{3+} ion can successfully substitute Al^{3+} site in YAG forming Ce^{3+}_{Al} center. It is known, that Al^{3+} sites in YAG have the nearest surroundings of two types: tetrahedral and octahedral. If the Ce^{3+} replaces the Al^{3+} ions, that are located in octahedral positions, it has 6-coordinated nearest surroundings, while tetrahedral Ce^{3+}_{Al} is 4-fold-coordinated. In any case Ce^{3+}_{Al} ion has another symmetry because regular Ce^{3+}_{Y} ion nearest surroundings is 12-fold-coordinated. It means that there is absolutely different crystal field splitting of 5d excited state for Ce^{3+}_{Al} and Ce^{3+}_{Y} centers. Hence, Ce^{3+}_{Al} and Ce^{3+}_{Y} centers have spectrally different emission bands: the blue-UV and yellow-green, respectively. The difference in the crystal field splitting for Ce^{3+}_{Al} and Ce^{3+}_{Y} centers is confirmed also by their excitation spectra (Fig. 2), which are absolutely different for different emission centers. The existence of two types of non-equivalent Al^{3+} sites in YAG means that there are two types of Ce^{3+}_{Al} centers in nanocrystals. It explains unusual broadening the blue-UV emission.

Since ionic radii of the aluminium and cerium are different (1.15 Å for Ce^{3+} and 0.675 Å for Al^{3+}) the formation of Ce^{3+}_{Al} in bulk YAG:Ce is impossible. However, in contrast to bulk YAG:Ce nanoparticles have a big surface area where a relatively large Ce^{3+} ion can successfully substitute Al^{3+} site on nanoparticle's surface. Surface origin of Ce^{3+}_{Al} in YAG:Ce nanocrystals is also confirmed by the following experimental facts: (i) there is a strong concentration quenching of the intensity of the blue-UV emission (Fig. 1(g–l)); (ii) there are unusual fast decay kinetics of the blue-UV emission (Fig. 3(b)) comparing with the regular yellow-green luminescence (Fig. 3(a)). Indeed, increasing Ce^{3+} concentration leads to the high concentration of Ce^{3+}_{Al} ions in restricted surface area creating favourable conditions for non-radiative cross-relaxation processes resulting to the degradation of the blue-UV emission band (see evolution in Fig. 1(g–l). Furthermore, nanoparticle's surface always has some amount of surface loss centers, which significantly increase the probability of non-radiative processes shortening emission decay time. Obviously, the influence of surface loss centers is stronger if luminescence centers are close to the nanoparticle's surface. Since the decay time of the blue-UV emission is much faster than the yellow-green one, we conclude that Ce^{3+}_{Al} centers stem from surface site or in the close vicinity of nanoparticle's surface. Note, the decay kinetics of the blue-UV emission do not contain any slow decay component similar to the decay time of the regular Ce^{3+} emission. It means that there are no Ce^{3+}_{Al} centers in volume of nanoparticles.

In order to confirm the suggested model of the emission center responsible for the intensive blue-UV emission there are several forthcoming research activities should be implemented. EPR, EXAFS of YAG:Ce nanocrystals definitely can highlight the local structure of the center responsible for the blue-UV emission, while luminescence studies of undoped YAG nanocrystals can elucidate the role of intrinsic defects. These forthcoming experiments can also elucidate the existence of another phase in nanocrystals. Microinclusions of perovskite phase in garnets are quite typical phenomena [31] and it can strongly influence luminescence properties of garnets.

3 Conclusion In conclusion, the intensive blue-UV emission has been discovered in nanocrystalline YAG:Ce. Analysing time-resolved luminescence characteristics obtained in a wide spectral range we suggested that Ce^{3+} ions substituting Al^{3+} in nanoparticle's surface are responsible for the blue-UV emission observed in YAG:Ce nanocrystals. Depending on Ce^{3+} concentration the intensity of the blue-UV emission can reach up to 75% of intensity of the regular yellow-green emission in YAG:Ce nanocrystals. Intensive blue-UV emission makes possible a utilizing of nanocrystalline YAG:Ce in radiation therapy. Both blue-UV and yellow-green emissions in nanocrystalline YAG:Ce cover spectral range from 350 nm to 650 nm providing unique opportunity for the fabrication of a new type of actual white luminescent material based on one type of impurity ion only.

Acknowledgements V.P. acknowledges the financial support from University of Oulu Strategic Funding, Research Council of Natural Sciences of the Academy of Finland. The experiments at DESY leading to these results have received funding from the European Community's Seventh Framework Programme (FP7/2007-2013) under grant agreement #226716. Authors are thankful to Dr. A. Kotlov (DESY) for his assistance during beamtime experiments. Authors also grateful to Prof. Wieslaw Strek for the providing the YAG:Ce nanopowders.

References

[1] S. Shionoya, W. M. Yen, and H. Yamamoto, Phosphor Handbook, 2nd ed. (CRC Press, Boca Raton, 2006).
[2] G. Blasse and B. C. Grabmaier, Luminescent Materials (Springer-Verlag, Berlin, Heidelberg, 1994).

[3] H. Goesmann and C. Feldmann, Angew. Chem. Int. Ed. Engl. **49**, 1362 (2010).
[4] Y.-T. Nien et al., Mater. Chem. Phys. **93**, 79 (2005).
[5] R. Asakura et al., J. Lumin. **127**, 416 (2007).
[6] S. A. Hassanzadeh-Tabrizi, Adv. Powd. Tech. **23**, 324 (2012).
[7] E. De la Rosa et al., Opt. Mater **27**, 1793 (2005).
[8] V. Pankratov et al., Radiat. Meas. **42**, 679 (2007).
[9] V. Pankratov et al., IEEE Trans. Nucl. Sci. **55**, 1509 (2008).
[10] R. Fedyk et al., Opt. Mater. **29**, 1252 (2007).
[11] R. Pazik et al., Opt. Mater. **30**, 714 (2008).
[12] V. Pankratov et al., Radiat. Meas. **45**, 392 (2010).
[13] Yu. Zorenko et al., J. Lumin. **131**, 17 (2011).
[14] Yu. Zorenko et al., J. Lumin. **114**, 85 (2005).
[15] J. A. Mares et al., Radiat. Meas. **42**, 533 (2007).
[16] V. Pankratov et al., J. Appl. Phys. **110**, 053522 (2011).
[17] V. Pankratov, et al., J. Lumin. **113**, 143 (2005).
[18] A. Kalinko et al., Cent. Eur. J. Phys. **9**, 432 (2011).
[19] A. I. Popov et al., Nucl. Instrum. Methods B **310**, 23 (2013).
[20] V. Pankratov et al., Radiat. Meas. **56**, 13 (2013).
[21] V. Pankratov et al., Phys. Rev. B **83**, 045308 (2011).
[22] V. Pankratov et al., J. Phys.: Condens. Matter **28**, 015301 (2016).
[23] G. Zimmerer, Radiat. Meas. **42**, 859 (2007).
[24] P. Mazur et al., Mater. Sci. Poland **23**, 261 (2005).
[25] P. A. Tanner et al., J. Phys.: Condens. Matter **19**, 216213 (2007).
[26] T. Tomiki et al., J. Phys. Soc. Jpn. **60**, 2437 (1991).
[27] T. Tomiki et al., J. Phys. Soc. Jpn. **61**, 2382 (1992).
[28] M. Kirm et al., ECS Proc. **99-40**, 113 (2000).
[29] K. Riwotzki et al., J. Phys. Chem. B **104**, 2824 (2000).
[30] V. Pankratov et al., Phys. Status Solidi B **247**, 2252 (2010).
[31] T. Yanagida et al., Opt. Mater. **35**, 2480 (2013).

Cent. Eur. J. Phys. • 9(2) • 2011 • 432-437
DOI: 10.2478/s11534-010-0108-7

VERSITA

Central European Journal of **Physics**

Electronic excitations in $ZnWO_4$ and $Zn_xNi_{1-x}WO_4$ ($x = 0.1 - 0.9$) using VUV synchrotron radiation

Research Article

Aleksandr Kalinko[1]*, Alexey Kotlov[2], Alexei Kuzmin[1]†, Vladimir Pankratov[1], Anatoli I. Popov[1,3], Liana Shirmane[1]

1 *Institute of Solid State Physics, University of Latvia, Kengaraga street 8, LV-1063, Riga, Latvia*

2 *Hamburger Synchrotronstrahlungslabor HASYLAB at Deutsches Elektronensynchrotron DESY, Notkestraße 85, Hamburg 22607, Germany*

3 *Institute Laue Langevin, 6 rue Jule Horovitz, 38042, Grenoble, France*

Received 21 June 2010; accepted 13 October 2010

Abstract: The photoluminescence spectra and luminescence excitation spectra of pure microcrystalline and nano-sized $ZnWO_4$ as well as the $Zn_xNi_{1-x}WO_4$ solid solutions were studied using vacuum ultraviolet (VUV) synchrotron radiation. The samples were also characterized by x-ray powder diffraction. We found that: (i) the shape of the photoluminescence band at 2.5 eV, being due to radiative electron transitions within the $[WO_6]^{6-}$ anions, becomes modulated by the optical absorption of Ni^{2+} ions in the $Zn_xNi_{1-x}WO_4$ solid solutions; and (ii) no significant change in the excitation spectra of $Zn_{0.9}Ni_{0.1}WO_4$ is observed compared to pure $ZnWO_4$. At the same time, a shift of the excitonic bands to smaller energies and a set of peaks, attributed to the one-electron transitions from the top of the valence band to quasi-localized states, were observed in the excitation spectrum of nano-sized $ZnWO_4$.

PACS (2008): 78.55.Hx, 81.07.Wx, 71.35.-y

Keywords: $ZnWO_4$ • $Zn_xNi_{1-x}WO_4$ solid solutions • tungstates • electronic excitations • luminescence • VUV spectroscopy

1. Introduction

Sanmartinite ($ZnWO_4$) belongs to a wide group of wolframite-type tungstates having the general formula AWO_4 with $A^{2+} = Mg^{2+}, Mn^{2+}, Fe^{2+}, Co^{2+}, Ni^{2+}, Zn^{2+}$, and Cd^{2+} [1]. It is a technologically important material, which finds applications such as scintillation detectors, laser-active hosts, optical fibers, sensors, and phase-change optical recording media [2–7]. In addition, $ZnWO_4$ shows highly efficient (> 50%) picosecond multiple Stokes and anti-Stokes generation when used as a Raman-active crystal in solid-state lasers, based on stimulated Raman scattering (SRS) [5, 8]. In the latter case, the strong SRS-active Raman mode at 907 cm^{-1} is

*E-mail: akalin@latnet.lv (Corresponding author)
†E-mail: a.kuzmin@cfi.lu.lv

the internal stretching W-O A_g-mode in the WO_6 octahedra [5, 8]. The tuning of the mode frequency can be achieved in tungstate solid solutions. Three such systems are known based on zinc tungstate: $ZnWO_4$-$FeWO_4$ [9], $ZnWO_4$-$MnWO_4$ [9], and $ZnWO_4$-$NiWO_4$ [10]. The latter system finds also application as a yellow ceramic pigment [10].

The optical and luminescent properties of wolframite-type $ZnWO_4$ have been widely studied in the past more than once. In particular, the intrinsic luminescence band, observed at room temperature at about 2.5 eV, has been attributed to a charge transfer between oxygen and tungsten ions in the $[WO_6]^{6-}$ anions [11–14]. The contributions from defects and distorted tungsten-oxygen octahedra have been also observed [15–17]. Up to now, most fundamental studies on tungstates have been performed on single-crystal samples. In this work we present the results on nano-sized $ZnWO_4$ and microcrystalline $Zn_xNi_{1-x}WO_4$ solid solutions using vacuum ultraviolet (VUV) synchrotron radiation spectroscopy.

2. Experiment

Pure $ZnWO_4$ and the solid solutions $Zn_xNi_{1-x}WO_4$ ($x = 0.1 - 0.9$) were synthesized using a co-precipitation technique [18, 19]. All chemicals used were analytic grade reagents (purity 99%, "Reahim") without further purification. Pure $ZnWO_4$ was prepared by the reaction of $ZnSO_4{\cdot}7H_2O$ and $Na_2WO_4{\cdot}2H_2O$ at room temperature (20°C), pH 8, and a reaction time of 1-2 hours. The water solutions of the two salts were prepared by dissolving 10 mmol of the salt in 100 ml of double-distilled water with vigorous stirring. Next they were mixed in 1:1 molar ratio, and white precipitates appeared immediately. After completion of the precipitate reaction, the precipitate was filtered off, washed several times with distilled water, and dried in air for 12 hours at 80°C thus resulting in the white-colored nano-sized $ZnWO_4$ powder [19]. Previous structural studies indicated that the $ZnWO_4$ powder as prepared has particles of size below 2 nm and a relaxed $ZnWO_4$ structure [19][1].

The nano-sized powder was next annealed in air for 4 hours at 400°C and 800°C. Annealing above 400°C results in the growth of crystallites, so that material becomes microcrystalline [19]. The yellow-colored solid solutions $Zn_xNi_{1-x}WO_4$ ($x = 0.1$–0.9) were prepared by first mixing proper amounts of water solutions of $ZnSO_4{\cdot}7H_2O$ and $Ni(NO_3)_2{\cdot}6H_2O$ salts and further following the same preparation procedure. After drying, the obtained solid solutions were annealed in air for 4 hours at 800°C.

The samples' crystallinity and phase composition (formation of solid solution) were controlled by x-ray powder diffraction (XRD). The XRD patterns (Fig. 1) were recorded at 20°C using a Bragg-Brentano powder diffractometer with a graphite monochromator in the diffracted beam to eliminate the specimen's fluorescence. A conventional tube with a copper anode (Cu $K\alpha$ radiation) was used as x-ray source. The measurements were performed in the angle range $2\theta = 5 - 70°$ with the step $\Delta(2\theta) = 0.05°$. The XRD data (ICSD No. 81937) for monoclinic ($P2/c$) $ZnWO_4$ from [20] were used for comparison.

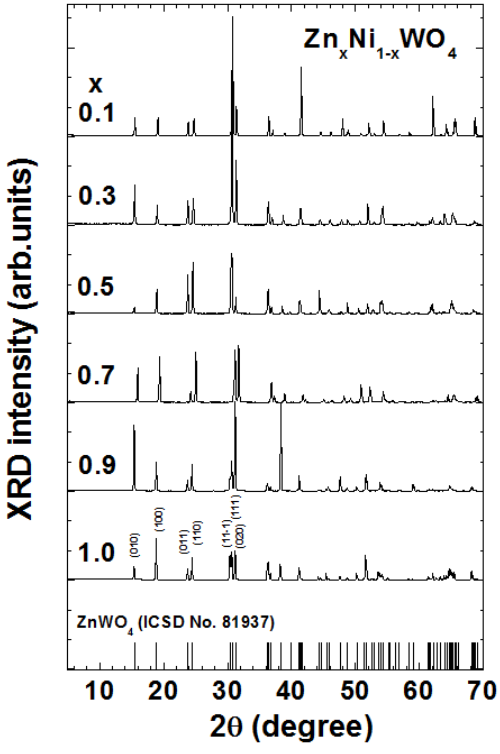

Figure 1. X-ray diffraction patterns of the microcrystalline $ZnWO_4$ and $Zn_xNi_{1-x}WO_4$ solid solutions annealed at 800°C. (Only a few patterns are shown for clarity).

The photoluminescence spectra were measured using pulsed YAG:Nd laser excitation (4.66 eV, 8 ns) at 20°C. The excitation spectra were collected at room temperature exploiting ultraviolet (UV) and vacuum ultraviolet (VUV) synchrotron radiation (3.6 – 20 eV) emitted from the DORIS III storage ring at the SUPERLUMI station

[1] A. Kuzmin, A. Kalinko, J. Timoshenko, HASYLAB Annual Report 2009: http://hasylab.desy.de/annual_report/files/2009/2009560.pdf

(HASYLAB DESY, Hamburg). The measurement procedure has been described in details elsewhere [21, 22].

Table 1. Lattice parameters (a, b, c, β) and unit cell volume (V) of monoclinic ($P2/c$) $ZnWO_4$ ($x = 1$) and $Zn_xNi_{1-x}WO_4$ ($x = 0.1 - 0.9$) solid solutions annealed at 800°C.

x	a (Å)	b (Å)	c (Å)	β (°)	V (Å^3)
1	4.69	5.72	4.93	90.7	132.4
0.9	4.69	5.73	4.94	90.5	132.9
0.8	4.67	5.69	4.93	90.3	131.1
0.7	4.67	5.70	4.92	90.4	130.9
0.6	4.68	5.70	4.94	90.5	131.5
0.5	4.66	5.70	4.93	90.2	131.1
0.4	4.65	5.70	4.93	90.0	130.7
0.3	4.64	5.69	4.93	90.1	130.3
0.1	4.61	5.68	4.92	90.0	129.0

3. Results and discussion

The XRD patterns in Fig. 1 indicate that pure $ZnWO_4$ and the $Zn_xNi_{1-x}WO_4$ solid solutions are formed after annealing at 800°C. The XRD pattern of pure $ZnWO_4$ was indexed using the standard data (Inorganic Crystal Structure Database (ICSD) No. 81937) for monoclinic ($P2/c$) $ZnWO_4$ from [20]. Upon substitution of Zn^{2+} by Ni^{2+} ions, the positions of the Bragg peaks in the XRD patterns shift slightly in the direction of larger scattering angles for increasing nickel content due to a decrease of the lattice parameters (Table 1). Upon increasing nickel content (x), the variation of the c parameter is small ($\sim$ 0.01 Å), but the values of the a and$b$ parameters decrease by $\sim$ 0.08 Å and $\sim$ 0.04 Å, respectively. Also the unit cell volume decreases from $V = 132.4$ Å^3 in $ZnWO_4$ to $V = 129.0$ Å^3 in $Zn_{0.1}Ni_{0.9}WO_4$. The results reported in Table 1 are in agreement with that found in the literature for pure tungstates ($ZnWO_4$ [10, 20] and $NiWO_4$ [23]) and $Zn_xNi_{1-x}WO_4$ solid solutions [10]. Note that the unit cell volume in $NiWO_4$ ($V = 127.7$ Å^3) [23] is expected to be smaller by only about 3.5% than that of $ZnWO_4$ ($V = 132.3$ Å^3) [20].

The phase of the $Zn_xNi_{1-x}WO_4$ solid solutions remains monoclinic wolframite-type, and the appearance of any other phases was not observed, in agreement with [10]. Such behaviour can be expected from the close size of Zn^{2+} and Ni^{2+} ions [24] and is in agreement with previous findings in [10]. Note that the Bragg peaks in the XRD patterns in Fig. 1, for example, the three Bragg peaks (11-1), (111), and (020) located at $2\theta = 31°$, are slightly better resolved than in [10].

The photoluminescence spectrum of pure $ZnWO_4$ powder consists of a broad band, peaked at about 2.5 eV (Fig. 2). When mixed with $NiWO_4$, the $Zn_xNi_{1-x}WO_4$ solid solutions are readily formed, and the luminescence spectrum splits into three sub-bands, centred at $\sim$ 2.26 eV, $\sim$ 2.5 eV, and $\sim$ 3.0 eV. Note that the photoluminescence spectra in Fig. 2 have been normalized at the band maximum, and their intensity should not be compared. In fact, addition of nickel results in a reduction of the total photoluminescence signal. We believe that the photoluminescence in the solid solutions has origin similar to that in pure $ZnWO_4$, however it is modulated by the self-absorption effect due to the presence of the Ni^{2+} ions.

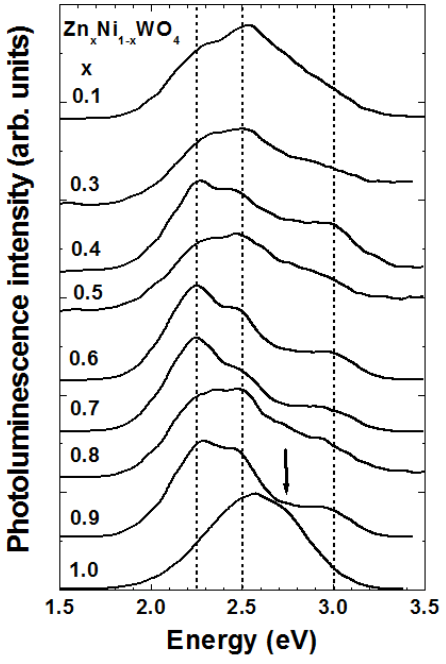

Figure 2. Photoluminescence of microcrystalline pure $ZnWO_4$ ($x = 1$) and the $Zn_xNi_{1-x}WO_4$ solid solutions annealed at 800°C.

In pure $ZnWO_4$ the origin of the main band at 2.5 eV has been previously assigned to radiative electron transitions within the $[WO_6]^{6-}$ anions [11, 12]. At the same time, the band at $\sim$ 2.3 eV has been attributed to recombination of e-h pairs localized at oxygen-atom-deficient tungstate ions [15, 16] or distorted WO_6 octahedra [17].

The origin of the last band at 3.0 eV appearing in the solid solutions is attributed to the interference between the broad luminescence band of the WO_6 groups and the absorption band of the NiO_6 groups. The self-absorption effect is caused by the intensive transition at $\sim$ 2.72 eV from the ground state $^3A_{2g}$ to the excited state $^3T_1$ of Ni^{2+} ($3d^8$) ions [10, 25] in distorted octahedral coordination [23].

The presence of this absorption band results in a notch at 2.7 eV in the emission band, thus making the peak at ~ 3.0 eV more pronounced.

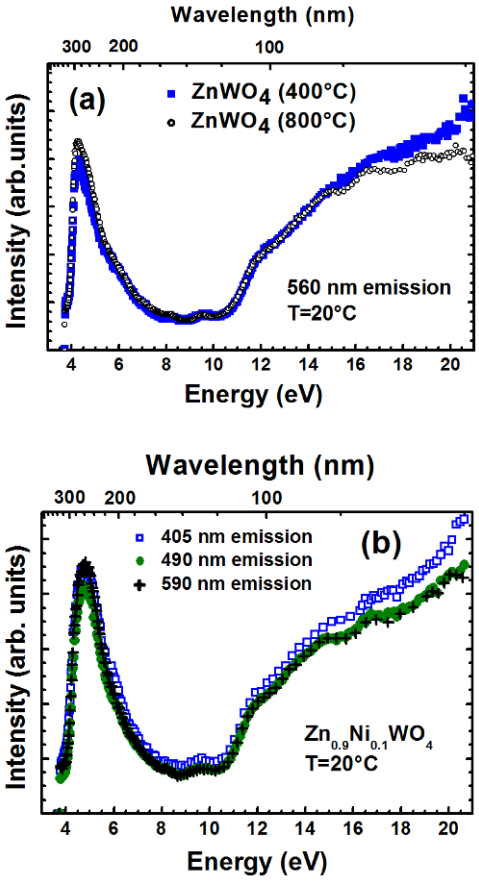

Figure 3. Room temperature (20°C) excitation spectra of pure $ZnWO_4$ and $Zn_{0.9}Ni_{0.1}WO_4$. (a) 560 nm emission in pure $ZnWO_4$, obtained from nano-sized $ZnWO_4$ by annealing at 400°C (solid squares) and 800°C (open circles). (b) 405 nm (open squares), 490 nm (solid circles) and 590 nm (crosses) emission in $Zn_{0.9}Ni_{0.1}WO_4$.

The excitation spectra are similar for pure $ZnWO_4$ and 10% Ni-doped $ZnWO_4$ powders (Fig. 3). They consists of a strong band at ~ 4.0 eV having the excitonic origin [11, 12]. The intensity of the excitation spectra starts to grow in the energy region above ~ 11 eV due to the beginning of the multiplication of electronic excitation (MEE) process [11, 12]. In this process, a secondary electron-hole (e-h) pair is created due to the inelastic scattering of a sufficiently 'hot' photoelectron, having an energy exceeding twice that of the band gap value. Further increase of the excitation energy results in deeper valence electrons starting to participate in the MEE process. Finally, when the photon energy reaches ~ 17 eV, i.e., $\approx 2E_g + E_V$ where

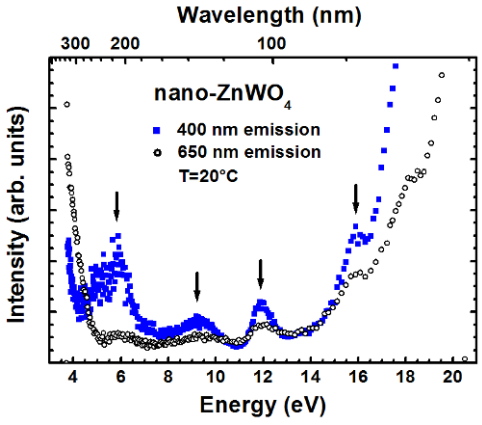

Figure 4. Room temperature (20°C) excitation spectra of the 400 nm and 650 nm emissions in pure as-prepared nano-sized $ZnWO_4$, dried in air for 12 hours at 80°C. The bands due to one-electron transitions are indicated by vertical arrows.

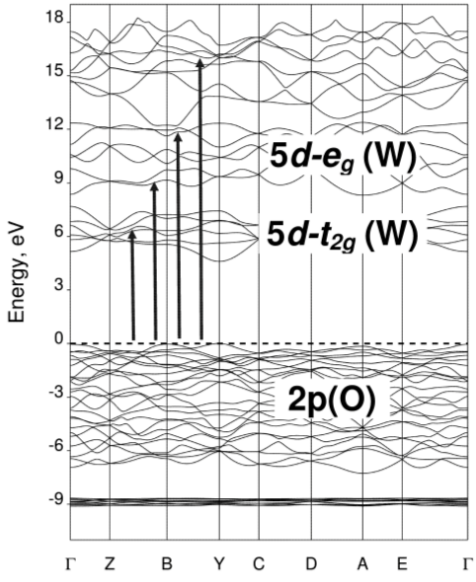

Figure 5. Band structure diagram for wolframite-type $ZnWO_4$ from [27]. The energy zero is set at the Fermi energy level. The one-electron transitions, corresponding to the peaks (see Fig. 4) in the excitation spectra of nano-sized $ZnWO_4$, are indicated by vertical arrows.

$E_g \approx 4.6 - 4.9$ eV is the band gap energy [11, 26, 27], and $E_V \approx 7.5$ eV (Fig. 5) is the valence band width [27], the electrons from the bottom of the valence band participate in the MEE process, and the intensity of the excitation spectra exhausts [11, 12]. Note also that the excitation spectra in Fig. 3 are weakly modulated by a fine structure

giving rise to several peaks at about 6, 8, 9.5, 12, 15, and 17 eV: among these the last four peaks are better visible. These energies correlate with the one-electron transitions from the top of the valence band to the conduction band as supported by our LCAO (linear combination of atomic orbitals) calculations [27].

The excitation spectra in nano-$ZnWO_4$ detected at 400 nm and 650 nm, are close to that from the crystal (Fig. 4). However, a strong band of the excitonic origin is shifted to smaller energies below $\sim$ 4.0 eV, due to a decrease of the optical band gap caused by disorder [28]. The presence of local structural relaxation in nano-$ZnWO_4$ is confirmed by the extended x-ray absorption fine structure (EXAFS) studies[2] and is in agreement with the recent Raman and luminescence results [19]. A set of peaks observed at 6, 9, 12, and 16 eV in Fig. 4 is attributed to the one-electron transitions from the top of the valence band to quasi-localized states. Such interpretation is in agreement with the first principles LCAO calculations [27] of the band structure for wolframite-type $ZnWO_4$ (Fig. 5). The LCAO calculations show that the valence band of $ZnWO_4$, having largely O 2p character, is separated by the band gap of 4.6 eV from the bottom of conduction band, which is dominated by W 5d states [27]. Therefore, the peaks located between 5 eV and 17 eV in excitation spectra of nano-$ZnWO_4$ (Fig. 4) are of charge transfer type from oxygen to tungsten.

4. Conclusions

The luminescence spectra and luminescence excitation spectra of pure microcrystalline and nano-sized $ZnWO_4$ and the $Zn_xNi_{1-x}WO_4$ solid solutions were studied using vacuum ultraviolet (VUV) synchrotron radiation.

The addition of nickel to $ZnWO_4$ increases the intensity of emission at $\sim$ 2.3 eV due to a distortion of WO_6 octahedra. The excitation spectra are similar in pure and $Zn_{0.9}Ni_{0.1}WO_4$ powders showing strong excitonic band at $\sim$ 4.0 eV and the effect from multiplication of electronic excitation (MEE) process above $\sim$ 11 eV.

The shift of the excitonic band in the excitation spectra of nanosized $ZnWO_4$ is caused by the local structural relaxation. In nanosized $ZnWO_4$, a number of bands is observed in the excitation spectra due to one-electron transitions from the top of the valence band to quasi-localized states.

[2] A. Kuzmin, A. Kalinko, J. Timoshenko, HASYLAB Annual Report 2009: http://hasylab.desy.de/annual_report/files/2009/2009560.pdf

Acknowledgements

This work was supported by ESF Project 2009/0202/1DP/1.1.1.2.0/09/APIA/VIAA/141, Latvian Government Research Grant No. 09.1518 and Joint Project No. 10.0032. The research leading to these results has also received funding from the European Community's Seventh Framework Programme (FP7/2007-2013) under grant agreement No. 226716.

References

[1] A.W. Sleight, Acta. Crystallogr. B 28, 2899 (1972)
[2] H. Wang, F.D. Medina, D.D. Liu, Y.D. Zhou, J. Phys.-Condens. Mat. 6, 5373 (1994)
[3] H. Kraus et al., Phys. Lett. B 610, 37 (2005)
[4] H. Grassmann, H.G. Moser, E. Lorenz, J. Lumin. 33, 21 (1985)
[5] A.A. Kaminskii, Appl. Optics 38, 4533 (1999)
[6] A.R. Phani, M. Passacantando, L. Lozzi, S. Santucci, J. Mater. Sci. 35, 4879 (2000)
[7] A. Kuzmin, R. Kalendarev, A. Kursitis, J. Purans, J. Non-Cryst. Solids 353, 1840 (2007)
[8] H.M. Pask, Prog. Quant. Electron. 27, 3 (2003)
[9] L.C. Hsu, Am. Mineral. 66, 298 (1981)
[10] A.L.M. de Oliveira et al., Dyes Pigments 77, 210 (2008)
[11] V.N. Kolobanov et al., Nucl. Instrum. Meth. A 486, 496 (2002)
[12] V. Nagirnyi et al., Nucl. Instrum. Meth. A 486, 395 (2002)
[13] V. Pankratov, L. Grigorjeva, D. Millers, S. Chernov, S. Voloshinovskii, J. Lumin. 94, 427 (2001)
[14] L. Grigorjeva, D. Millers, S. Chernov, V. Pankratov, A. Watterich, Radiat. Meas. 33, 645 (2001)
[15] M. Itoh, T. Katagiri, T. Aoki, M. Fujita, Radiat. Meas. 42, 545 (2007)
[16] Z. Lou, J. Hao, M. Cocivera, J. Lumin. 99, 349 (2002)
[17] V.B. Mikhailik, H. Kraus, G. Miller, M.S. Mykhaylyk, D. Wahl, J. Appl. Phys. 97, 083523 (2005)
[18] G. Huang, Y. Zhu, Mater. Sci. Eng. B-Adv. 139, 201 (2007)
[19] A. Kalinko, A. Kuzmin, J. Lumin. 129, 1144 (2009)
[20] P.F. Schofield, K.S. Knight, G. Cressey, J. Mater. Sci. 31, 2873 (1996)
[21] G. Zimmerer, Radiat. Meas. 42, 859 (2007)
[22] V. Pankratov, M. Kirm, H. von Seggern, J. Lumin. 113, 143 (2005)
[23] H. Weitzel, Z. Kristallogr. 144, 238 (1976)
[24] R.D. Shannon, Acta Crystallogr. A 32, 751 (1976)
[25] L.N. Limarenko, A.E. Nosenko, M.V. Pashkovskii,

D.-L.L. Futorskii, Influence of structural defects on physical properties of tungstates. (Vysha Shkola, Lvov, 1978)

[26] M. Itoh, N. Fujita, Y. Inabe, J. Phys. Soc. Jpn. 75, 084705 (2006)

[27] A. Kalinko, A. Kuzmin, R.A. Evarestov, Solid State Commun. 149, 425 (2009)

[28] E. Orhan et al., J. Solid State Chem. 178, 1284 (2005)

UV-VUV synchrotron radiation spectroscopy of $NiWO_4$

A. Kuzmin[a)]

Institute of Solid State Physics, University of Latvia, 8 Kengaraga str., LV-1063 Riga, Latvia

V. Pankratov

Institute of Solid State Physics, University of Latvia, 8 Kengaraga str., LV-1063 Riga, Latvia and Research Center of Molecular Materials, University of Oulu, P.O. Box 3000, FIN-90014 Oulu, Finland

A. Kalinko

Institute of Solid State Physics, University of Latvia, 8 Kengaraga str., LV-1063 Riga, Latvia and DESY Photon Science, Notkestraße 85, D-22607 Hamburg, Germany

A. Kotlov

DESY Photon Science, Notkestraße 85, D-22607 Hamburg, Germany

L. Shirmane and A. I. Popov

Institute of Solid State Physics, University of Latvia, 8 Kengaraga str., LV-1063 Riga, Latvia

(Submitted January 18, 2016)
Fiz. Nizk. Temp. **42**, 694–698 (July 2016)

Photoluminescence and excitation spectra of microcrystalline and nanocrystalline nickel tungstate ($NiWO_4$) were measured using UV-VUV synchrotron radiation source. The origin of the bands is interpreted using comparative analysis with isostructural $ZnWO_4$ tungstate and based on the results of recent first-principles band structure calculations. The influence of the local atomic structure relaxation and of Ni^{2+} intra-ion *d–d* transitions on the photoluminescence band intensity are discussed. *Published by AIP Publishing*. [http://dx.doi.org/10.1063/1.4959010]

Introduction

Metal tungstates (MWO_4) have received considerable interest from both theoretical and technological point of view due to their excellent combination of the optical, piezoelectric, ferroelectric and other properties.[1,2] The optical properties of different metal tungstates can be controlled by their composition and many wide band-gap tungstates are found to be promising materials for scintillator applications.[3–10]

Among them, nickel tungstate ($NiWO_4$) finds applications in catalysis,[11–14] as humidity[15] and gas[16] sensor, a photoanode in photovoltaic electrochemical cell,[17] a pigment[18] and in microwave[19] and electrochromic[20,21] devices. These applications are tightly connected to its electronic structure being scarcely studied in the past. The electronic band structure of $NiWO_4$ was calculated recently using first-principles spin-polarized periodic linear combination of atomic orbitals (LCAO) method in Ref. 22. The photoluminescence properties of $NiWO_4$ powder and sol-gel derived $NiWO_4$ films, calcined above 600 °C, were investigated at room temperature under pulsed Xenon discharge lamp excitation in Ref. 23, indicating the presence of a broad blue-green (2.07–3.54 eV) photoluminescence band.

In this work, we present original results on the photoluminescence and excitation spectra of microcrystalline and nanocrystalline $NiWO_4$, obtained using UV-VUV synchrotron radiation spectroscopy. The experiments were carried out at SUPERLUMI beamline (HASYLAB at DESY, Hamburg) using 4–20 eV synchrotron radiation from the DORIS storage ring for excitation.[24] This experimental set-up is a unique tool for investigations of different types of wide band gap materials.[24–33] The interpretation of the photoluminescence and excitation spectra is given based on the comparative analysis with isomorphous $ZnWO_4$ tungstate[32] and using the results of LCAO calculations[22] and the Ni(Zn) *K*-edge and W L_3-edge x-ray absorption spectroscopy studies.

Experimental and calculation details

$NiWO_4$ and $ZnWO_4$ powders were synthesized using coprecipitation technique by mixing two aqueous solutions of Na_2WO_4–$2H_2O$ and $Ni(NO_3)_2 \cdot 6H_2O$ or $ZnSO_4 \cdot 7H_2O$ salts in bi-distilled water at room temperature (20 °C). The pH value of the solution was equal to eight. The tungstate sediment was subsequently washed, filtrated and, after drying, annealed in air for 4 h at 80 °C (nanocrystalline sample with crystallites size below 2 nm) and 900 °C (microcrystalline sample). More details can be found in Ref. 32.

The photoluminescence (Fig. 1) and excitation (Fig. 2) spectra were collected at 7–300 K exploiting ultraviolet (UV) and vacuum ultraviolet (VUV) synchrotron radiation (3.6–20.0 eV) emitted from DORIS III storage ring at SUPERLUMI station (HASYLAB DESY, Hamburg).

The low-temperature (10 K) Ni(Zn) *K*-edge and W L_3-edge x-ray absorption spectra were measured in transmission mode at the HASYLAB/DESY C bending-magnet beamline. The x-ray radiation was monochromatized by a detuned Si(111) double-crystal monochromator, and the beam intensity was measured using two ionization chambers filled with argon and krypton gases. The x-ray absorption spectra were

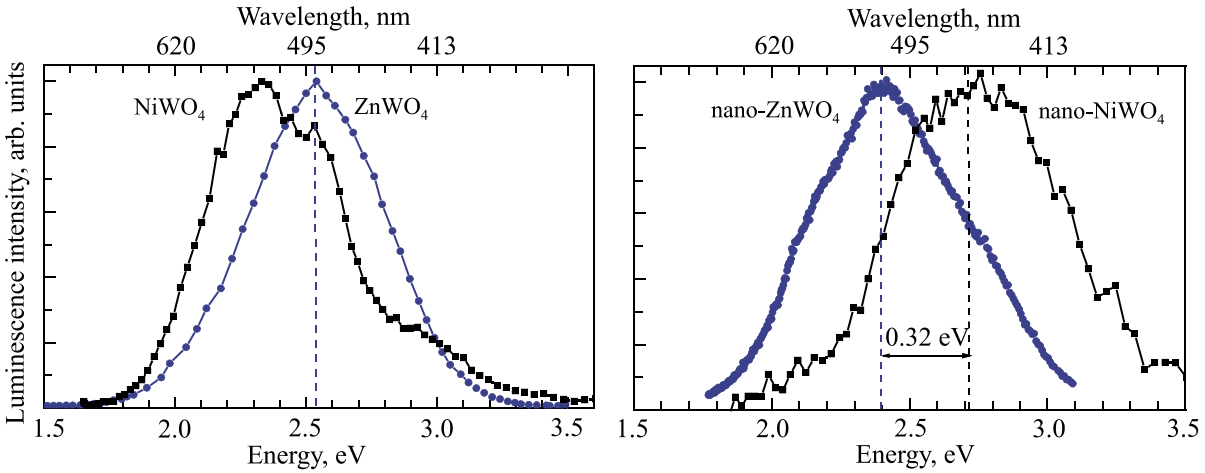

FIG. 1. The photoluminescence spectra of microcrystalline (left panel) and nanocrystalline (right panel) Ni(Zn)WO_4 powders excited by 13.8 eV photons.

analyzed using the EDA software package[34] following conventional procedure.[35] Radial distribution functions (RDFs) $G(R)$ (Fig. 3) for Ni(Zn)–O and W–O bonds in microcrystalline and nanocrystalline Ni(Zn)WO_4 were obtained by the regularization-like method[34,36,37] from the Ni(Zn) K-edge and W L_3-edge extended x-ray absorption fine structure (EXAFS) spectra. Theoretical scattering amplitude and phase shift functions, employed in the EXAFS simulations, were calculated for $NiWO_4$ and $ZnWO_4$ crystallographic structures by the *ab initio* FEFF8 code[38,39] using complex exchange-correlation Hedin–Lundqvist potential.

Results and discussion

Photoluminescence spectra

Both tungstates $NiWO_4$ and $ZnWO_4$ have monoclinic wolframite-type structure (space group $P2/c$) with two formula units ($Z = 2$) per primitive cell.[40] All metal atoms (Ni, Zn, and W) are six-fold octahedrally coordinated by oxygen atoms. The presence of two non-equivalent oxygen atoms results in metal-oxygen octahedron distortion,[41] which is the largest for WO_6 octahedron and the smallest for NiO_6 octahedron (Fig. 3).

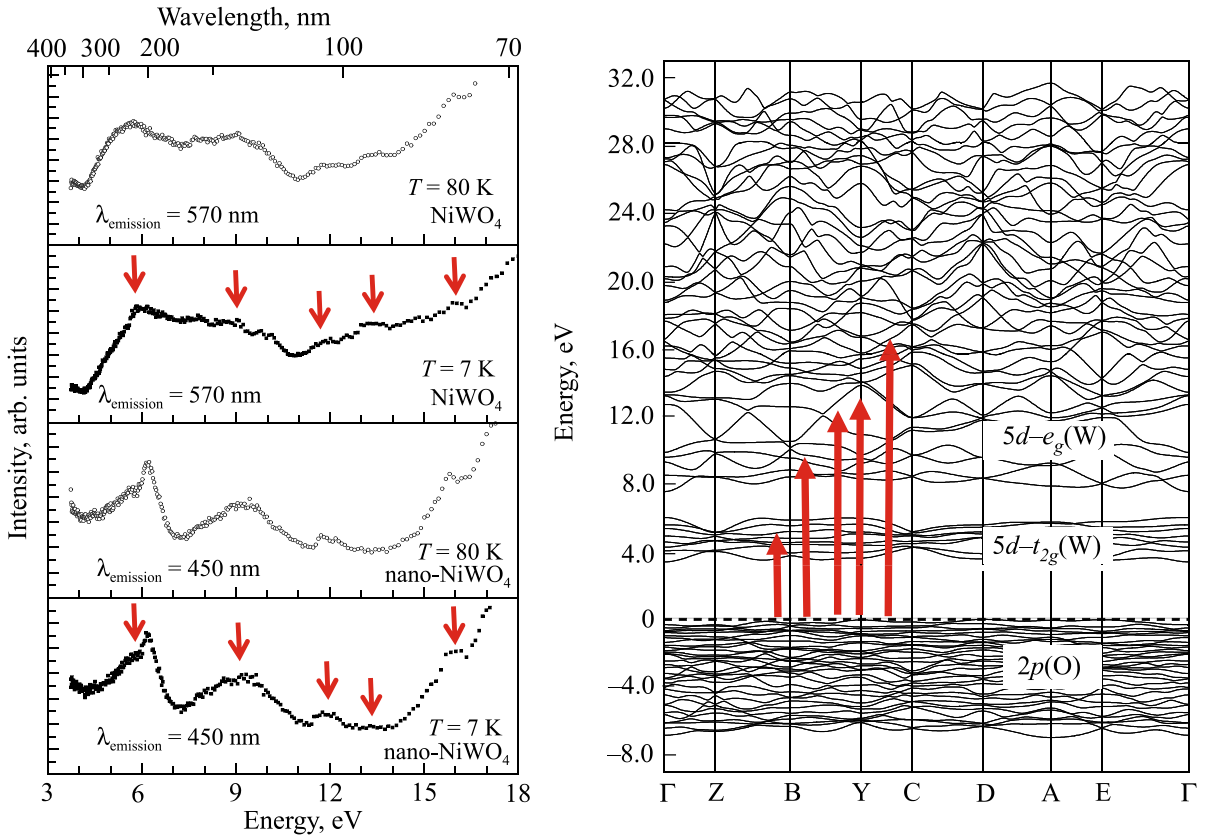

FIG. 2. Left panel: Excitation spectra of microcrystalline and nanocrystalline $NiWO_4$ at $T = 7$ and 80 K. The bands due to the one-electron transitions are indicated by vertical arrows. Right panel: Electronic band structure diagram for wolframite-type $NiWO_4$ from Ref. 22. The energy zero is set at the Fermi-energy level. The one-electron transitions, corresponding to the peaks at 6, 9, 12, 13.5, and 16 eV in the excitation spectrum of $NiWO_4$ are indicated by vertical arrows.

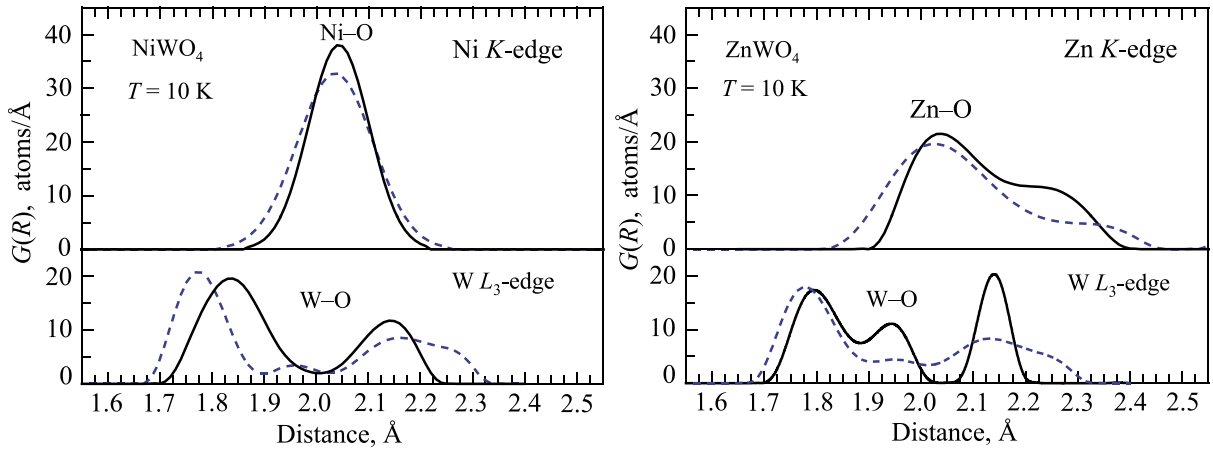

FIG. 3. Radial distribution functions (RDFs) $G(R)$ for Ni(Zn)–O and W–O bonds within the first coordination shells of metal atoms in microcrystalline (solid lines) and nanocrystalline (dashed lines) Ni(Zn)WO_4, obtained from the analysis of the Ni(Zn) K-edge and W L_3-edge EXAFS spectra at 10 K.

The photoluminescence spectrum of microcrystalline $ZnWO_4$ powders consists of a broad band, peaked at about 2.5 eV (Fig. 1). The origin of the band has been previously assigned to radiative electron transitions within the $[WO_6]^{6-}$ molecular complex.[42,43] In $NiWO_4$, the same photoluminescence band has irregular asymmetric shape, which is close to that observed previously in solid solutions $Zn_cNi_{1-c}WO_4$.[32] The origin of such band shape can be attributed[32] to the self-absorption effect, i.e., to a modulation of optical absorption by the intense intra-ion transition within Ni^{2+} ($3d^8$) ions from the ground state[3] A_{2g} to the excited state[3] T_1.[44]

The maximum of the photoluminescence band in nano-$NiWO_4$ is located at 2.7 eV, thus being shifted by ~0.32 eV to higher energy compared to nano-$ZnWO_4$.[45] Such blue-shift can be explained by a difference in the relaxation of WO_6 octahedra in the two tungstates, which is directly evidenced by our W L_3-edge EXAFS data (Fig. 3).

Radial distribution functions $G(R)$ for Ni/Zn–O and W–O bonds in microcrystalline and nanocrystalline Ni(Zn)WO_4 are shown in Fig. 3. The shape of the RDFs confirms unambiguously that the WO_6 octahedra in both tungstates are strongly distorted. The relaxation of the first shell WO_6 and Ni(Zn)O_6 octahedra in nanocrystalline Ni(Zn)WO_4 is clearly observed. Note that in the case of WO_6 octahedra the relaxation affects both shortest (at 1.8–1.9 Å) and longest (at 2.1–2.2 Å) W–O bonds. The nearest group of the W–O bonds relaxes stronger in $NiWO_4$ (by ~0.07 Å) than in $ZnWO_4$ (by ~0.02 Å), thus being responsible for a difference in the position of the photoluminescence bands in the two nanotungstates.

Finally, we would like to note that no significant temperature effect has been observed on the photoluminescence spectra of microcrystalline and nanocrystalline $NiWO_4$ in the temperature range 7–80 K. Also the photoluminescence spectra of micro-$NiWO_4$ at $T = 80$ K show weak dependence on the excitation wavelength (4.96 or 13.8 eV).

Excitation spectra

The excitation spectra of microcrystalline $NiWO_4$ show some temperature dependence in the range from 7 to 80 K due to the lattice expansion (left panel in Fig. 2). They differ from that for $ZnWO_4$ from Ref. 32 due to the difference of about 1 eV in the band gaps: $E_g = 3.6$ eV (Ref. 46) for $NiWO_4$, but $E_g = 4.6$ eV for $ZnWO_4$.[47] As a result, the strong excitonic band clearly visible at ~4.5 eV for $ZnWO_4$ (Ref. 32) is not observed in the present data for $NiWO_4$ due to the spectrometer range limitations: the excitonic band is expected to be located below 3.7 eV.

The interpretation of the excitation spectra can be done using the electronic band structure diagram calculated for $NiWO_4$ in Ref. 22 using the first-principles spin-polarized periodic linear combination of atomic orbital (LCAO) method. The valence band of $NiWO_4$ is dominated by oxygen 2p-states hybridized with nickel $3d(t_{2g}, e_g\uparrow)$-states, whereas tungsten 5d-states and nickel $3d(e_g\downarrow)$-states contribute largely into the bottom of conduction band.[22]

The broad bands at 5–6, 8–10, 12, 13.5, and 16 eV are due to the one-electron transitions (arrows in the right panel of Fig. 2) from the top of the valence band. These transitions are even more pronounced in the case of nano-$NiWO_4$ due to quasi-localized nature of the involved electronic states. Note that such transitions have been also observed previously in nano-$ZnWO_4$.[32]

Conclusions

Microcrystalline and nanocrystalline $NiWO_4$ powders were studied by UV-VUV synchrotron radiation spectroscopy in comparison with isomorphous $ZnWO_4$ tungstate. The photoluminescence and excitation spectra were interpreted using the results of the first-principles LCAO calculations[22] and the local structural information from the Ni(Zn) K-edge and W L_3-edge x-ray absorption spectroscopy studies.

Similar to the case of $ZnWO_4$,[42,43] the photoluminescence spectra of both microcrystalline and nanocrystalline $NiWO_4$ powders originate in the $[WO_6]^{6-}$ molecular complex. However, their intensity is strongly modulated by the optical absorption of Ni^{2+} ions (intra-ion d–d transitions). In nano-$NiWO_4$, the photoluminescence band maximum is shifted to shorter wavelengths due to the strong relaxation of WO_6 octahedra.

The excitation spectra are similar in microcrystalline and nanocrystalline $NiWO_4$ powders. They consist of a number of bands due to the one-electron transitions across the band gap from the top of the valence band to the electron states in the conduction band and above. The bands are more

pronounced in nano-$NiWO_4$ due to quasi-localized character of the involved electronic states.

This work was supported by Latvian Science Council Grant No. 187/2012. The experiments at DESY leading to these results have received funding from the European Community's Seventh Framework Programme (FP7/2007-2013) under Grant Agreement No. 226716. V.P. acknowledges the financial supports from Oulu University Strategic Funding and Research Council for Natural Sciences of the Academy of Finland.

[a)]Email: a.kuzmin@cfi.lu.lv

[1]B. I. Kidyarov and V. V. Atuchin, Ferroelectrics **444**, 144 (2013).
[2]V. A. Isupov, Ferroelectrics **322**, 83 (2005).
[3]P. Lecoq, I. Dafinei, E. Auffray, M. Schneegans, M. V. Korzhik, O. V. Missevitch, V. B. Pavlenko, A. A. Fedorov, A. N. Annenkov, V. L. Kostylev, and V. D. Ligun, Nucl. Instrum. Methods Phys. Res. A **365**, 291 (1995).
[4]M. Kobayashi, M. Ishii, Y. Husuki, and H. Yahag, Nucl. Instrum. Methods Phys. Res. A **333**, 429 (1993).
[5]V. Nagirnyi, A. Kotlov, L. Jönsson, M. Kirm, and A. Lushchik, Nucl. Instrum. Methods Phys. Res. A **537**, 61 (2005).
[6]V. Nagirnyi, M. Kirm, A. Kotlov, A. Lushchik, and L. Jönsson, J. Lumin. **102–103**, 597 (2003).
[7]V. Nagirnyi, E. Feldbach, L. Jönsson, M. Kirm, A. Kotlov, A. Lushchik, L. L. Nagornaya, F. Savikhin, and G. Svensson, Radiat. Meas. **33**, 601 (2001).
[8]E. Feldbach, L. Jönsson, M. Kirm, A. Kotlov, A. Lushchik, V. Nagirnyi, G. Svensson, and M. Åsberg-Dahlborg, J. Lumin. **87–89**, 1213 (2000).
[9]D. Millers, S. Chernov, L. Grigorjeva, A. Popov, E. Auffray, I. Dafinei, P. Lecoq, and M. Schneegans, J. Lumin. **72–74**, 693 (1997).
[10]D. Millers, L. Grigorjeva, S. Chernov, A. Popov, P. Lecoq, and E. Auffray, Phys. Status Solidi B **203**, 585 (1997).
[11]F. J. Gil-Llambias, H. Rodriguez, I. Bouyssiers, M. Escudey, and I. Carkovic, J. Catal. **102**, 37 (1986).
[12]B. Scheffer, P. Molhoek, and J. A. Moulijn, Appl. Catal. **46**, 11 (1989).
[13]R. A. Diaz-Real, R. S. Mann, and I. S. Sambi, Ind. Eng. Chem. Res. **32**, 1354 (1993).
[14]D. L. Stern and R. K. Grasselli, J. Catal. **167**, 570 (1997).
[15]A. K. Bhattacharya, R. G. Biswas, and A. Hartridge, J. Mater. Sci. **32**, 353 (1997).
[16]V. Dusastre and D. E. Williams, J. Mater. Chem. **9**, 965 (1999).
[17]P. S. Pandey, N. S. Bhave, and R. B. Kharat, Electrochim. Acta **51**, 4659 (2006).
[18]A. L. M. de Oliveira, J. M. Ferreira, M. R. S. Silva, G. S. Braga, L. E. B. Soledade, M. A. M. M. Aldeiza, C. A. Paskocimas, S. J. G. Lima, E. Longo, A. G. de Souza, and I. M. G. dos Santos, Dyes Pigm. **77**, 210 (2008).
[19]R. C. Pullar, S. Farrah, and N. McN. Alford, J. Eur. Ceram. Soc. **27**, 1059 (2007).
[20]A. Kuzmin, J. Purans, R. Kalendarev, D. Pailharey, and Y. Mathey, Electrochim. Acta **46**, 2233 (2001).
[21]S. V. Green, A. Kuzmin, J. Purans, C. G. Granqvist, and G. A. Niklasson, Thin Solid Films **519**, 2062 (2011).
[22]A. Kuzmin, A. Kalinko, and R. A. Evarestov, Cent. Eur. J. Phys. **9**, 502 (2011).
[23]H. He, Int. J. Mater. Res. **101**, 386 (2010).
[24]G. Zimmerer, Radiat. Meas. **42**, 859 (2007).
[25]M. Kirm, E. Feldbach, T. Karner, A. Lushchik, Ch. Lushchik, A. Maaroos, V. Nagirnyi, and I. Martinson, Nucl. Instrum. Methods B **141**, 431 (1998).
[26]S. Nakonechnyi, T. Karner, A. Lushchik, C. Lushchik, V. Babin, E. Feldbach, I. Kudryavtseva, P. Liblik, L. Pung, and E. Vasil'chenko, J. Phys.: Condens. Matter **18**, 379 (2006).
[27]A. I. Popov, L. Shirmane, V. Pankratov, A. Lushchik, A. Kotlov, V. E. Serga, L. D. Kulikova, G. Chikvaidze, and J. Zimmermann, Nucl. Instrum. Methods B **310**, 23 (2013).
[28]P. V. Savchyn, V. V. Vistovskyy, A. S. Pushak, A. S. Voloshinovskii, A. V. Gektin, V. Pankratov, and A. I. Popov, Nucl. Instrum. Methods B **274**, 78 (2012).
[29]V. Pankratov, A. I. Popov, L. Shirmane, A. Kotlov, G. A. Bizarri, A. Burger, P. Bhattacharya, E. Tupitsyn, E. Rowe, V. M. Buliga, and R. T. Williams, Radiat. Meas. **56**, 13 (2013).
[30]E. Shablonin, A. I. Popov, A. Lushchik, A. Kotlov, and S. Dolgov, Physica B **477**, 133 (2015).
[31]E. V. Savchenko, G. Zimmerer, and V. E. Bondybey, J. Lumin. **129**, 1866 (2009).
[32]A. Kalinko, A. Kotlov, A. Kuzmin, A. Pankratov, A. I. Popov, and L. Shirmane, Cent. Eur. J. Phys. **9**, 432 (2011).
[33]N. B. Gruzdev, V. I. Sokolov, V. A. Pustovarov, and V. N. Churmanov, Fiz. Nizk. Temp. **41**, 285 (2015) [Low Temp. Phys. **41**, 218 (2015)].
[34]A. Kuzmin, Physica B **208–209**, 175 (1995).
[35]V. L. Aksenov, M. V. Kovalchuk, A. Yu. Kuzmin, Yu. Purans, and S. I. Tyutyunnikov, Crystallogr. Rep. **51**, 908 (2006).
[36]A. Kuzmin and J. Purans, J. Phys.: Condens. Matter **12**, 1959 (2000).
[37]A. Anspoks, A. Kalinko, J. Timoshenko, and A. Kuzmin, Solid State Commun. **183**, 22 (2014).
[38]A. L. Ankudinov, B. Ravel, J. J. Rehr, and S. D. Conradson, Phys. Rev. B **58**, 7565 (1998).
[39]J. J. Rehr and R. C. Albers, Rev. Mod. Phys. **72**, 621 (2000).
[40]H. Weitzel, Z. Kristallogr. **144**, 238 (1976).
[41]A. Kuzmin and J. Purans, Radiat. Meas. **33**, 583 (2001).
[42]V. N. Kolobanov, I. A. Kamenskikh, V. V. Mikhailin, I. N. Shpinkova, D. A. Spassky, B. I. Zadneprovsky, L. I. Potkin, and G. Zimmerer, Nucl. Instrum. Methods Phys. Res. A **486**, 496 (2002).
[43]V. Nagirnyi, E. Feldbach, L. J'onson, M. Kirm, A. Lushchik, V. A. Nefedov, and B. I. Zadneprovski, Nucl. Instrum. Methods Phys. Res. A **486**, 395 (2002).
[44]L. N. Limarenko, A. E. Nosenko, M. V. Pashkovskii, and D. L. L. Futorskii, *Influence of Structural Defects on Physical Properties of Tungstates* (Vysha Shkola, Lvov, 1978).
[45]A. Kalinko and A. Kuzmin, J. Lumin. **129**, 1144 (2009).
[46]T. Ejima, T. Banse, H. Takatsuka, Y. Kondo, M. Ishino, N. Kimura, M. Watanabe, and I. Matsubara, J. Lumin. **119–120**, 59 (2006).
[47]A. Kalinko, A. Kuzmin, and R. A. Evarestov, Solid State Commun. **149**, 425 (2009).

This article was published in English in the original Russian journal. Reproduced here with stylistic changes by AIP Publishing.